Florian Müller

Numerical Simulations of Fluorescence Recovery After Photobleaching Experiments

Diplomarbeit
zur Erlangung des akademischen Grades
Magister der Naturwissenschaften

Institut für Experimentalphysik
Karl Franzens Universität Graz
Universitätsplatz 5, 8010 Graz

Begutachter:
Univ. Prof. Dr.phil Max E. Lippitsch

Graz, Mai 2005

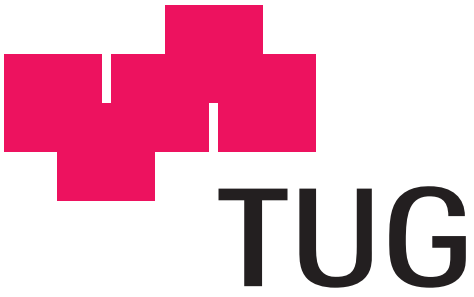

Institute for Genomics and Bioinformatics,
Graz University of Technology
Petersgasse 14, 8010 Graz, Austria
Head: Univ.-Prof. Dipl.-Ing. Dr.techn. Zlatko Trajanoski

Most of the research for this thesis was conducted under the supervision of DI Dr. Bernd Messnarz at the Institute for Genomics and Bioinformatics.

Abstract

Fluorescence Recovery After Photobleaching (FRAP) is a well established technique in molecular biology to investigate the biophysical properties of proteins in living cells. The reaction-diffusion equations that describe the protein dynamics during a FRAP experiment can be solved analytically only for idealized experimental geometries. The specific aims of this thesis were to solve these equations for realistic geometries. For these purposes a graphical user interface for the exact definition of the experiment was developed in MATLAB®. The differential equations were solved with an implementation of the finite element method (FEM) which was chosen because of its flexibility. It can be shown that a high accuracy of the numeric results can be obtained with selective refinement of the finite elements. Simulations with different experimental geometries and different bleaching patterns showed that changes in the experimental setup influence the results significantly. Ignoring these influences when working with experimental data would lead to a misinterpretation and a wrong estimation of the underlying parameters.

Keywords:
FRAP; Protein dynamics; Reaction-diffusion equation; Mathematical modeling; Simulation

Zusammenfassung

Fluorescence Recovery After Photobleaching (FRAP) ist eine etablierte Methode in der molekularen Zellbiologie zur Bestimmung der biophysikalischen Eigenschaften von Proteinen. Die Reaktions-Diffusions-Gleichungen, die die Proteindynamik während eines FRAP Experimentes beschreiben, sind analytisch jedoch nur für idealisierte experimentelle Geometrien lösbar. Ziel der Diplomarbeit war es, diese Gleichungen für realistische Geometrien zu lösen. Zu diesem Zweck wurde eine grafische Benutzeroberfläche zur exakten Definition des Experimentes mit dem Softwarepaket MATLAB® entwickelt. Als Lösungsmethode für die Differentialgleichungen wurde, aufgrund ihrer Flexibilität, die Implementierung der Finiten Elemente Methode (FEM) gewählt. Es konnte gezeigt werden, dass durch eine selektive Verfeinerung von finiten Elementen eine sehr hohe Genauigkeit der numerischen Lösung erzielt werden kann. Simulationen mit verschiedenen experimentellen Geometrien und unterschiedlichen Bleaching Mustern ergaben, dass diese Änderungen im experimentellen Aufbau die simulierten Daten stark beeinflussen. Eine Vernachlässigung dieser Einflüsse bei experimentellen Daten würde zu einer Fehlinterpretation der Daten und einer fehlerhaften Bestimmung der zugrunde liegenden Parameter führen.

Stichwörter:
FRAP; Proteindynamik; Reaktions-Diffusions Gleichung; Mathematische Modellierung; Simulation

Contents

List of Figures

List of Tables

Chapter 1

Introduction

Photobleaching experiments like FRAP (Fluorescence Recovery after Photobleaching) are a well established technique. Upon their development in the 70's these methods were primarily used to determine diffusion constants of biomolecules in membranes. Recently, with the development and use of fluorescent proteins as fusion tags to track protein behavior in living cells, complete new questions can be addressed. Photobleaching experiments together with kinetic modeling approaches allow us not only to assess the diffusion constant, but also the binding rates [9, 10, 32]. But even the kinetic model that describes the simplest realistic case of binding, namely a single binding interaction in the presence of cellular diffusion, can't be solved analytically in a general context. Several assumptions have to be met to make an analytical solution possible. The big advantages of these approaches are that the underlying biological model can be tested on the measured data, and the corresponding biophysical parameters can be estimated with data-fitting tools. These solutions are, however, restricted to problems described by simple geometries. Hence no information can be gathered about the impact of different geometries on the behavior of the recovery curve.

Therefore, I have developed a MATLAB®[1] environment, named *FrapSim*, for numerical simulations and analysis of photobleaching experiments. The kinetic model, that describes the time-dependent behavior of the biomolecules of interest, can be expressed in terms of a system of partial differential equations (PDE). There are numerous ways to solve such problems numerically. I choose an approach based on the Finite Element Method (FEM) because it is suitable for two main reasons. First, FEM are very flexible as far as the definition of the geometry of the problem is concerned. Second, Matlab provides with the PDE Toolbox an extensive tool for the study and

[1]Matlab is a registered trademark of The Mathworks, Inc. [33].

solution of PDE problems, which can be implemented in own applications. *FrapSim* has a graphical user interface that allows the user the specification of the whole photobleaching experiment. It is important to mention that with this numeric method no data-fitting can be performed.

The objectives of the *FrapSim* environment are to provide a tool to

- define a photobleaching experiment as a PDE problem, e.g., define 2-D geometries, PDE coefficients, and initial conditions,
- numerically solve the PDE problem,
- visualize and analyze the results.

Outline of the thesis

In the chapter *Basics* the most important fundamentals underlying a FRAP experiment are presented. It starts with an outline of the main properties of nuclear proteins in living cells, followed by an introduction into the most important experimental basics, which are essential to understand the principles underlying a FRAP experiment. The last section covers the definition of a mathematical model that describes the dynamics of nuclear proteins during such an experiment. The numeric solution is calculated with the finite element method (FEM). The basic of this method and the implementation in the *FrapSim* environment are presented in the chapter *Methods*. The first important step after the development of the simulation environment was the validation of the developed program in order to guarantee that the numeric results are accurate, which is presented in the first part of the *Results and discussion* chapter. The validation was done by comparing the numeric results to the results of an analytic model. The most promising strategy to obtain accurate results is described in the concluding remark. In the second part the results of simulations with different experimental setups are summarized. Changes in the experimental geometries can have a not negligible influence on the simulated results. Ignoring this influence during the evaluation of experimental data would lead to a misinterpretation of the data.

Chapter 2

Basics

The most important basics which are important to understand FRAP experiments are derived. The first section gives a brief introduction into protein dynamics and the architecture of the cell nucleus. The following section covers the experimental basics, that are crucial to understand how a FRAP experiment is performed. In the last section mathematical models describing the dynamics of proteins during a FRAP experiment are derived, and an analytical solution is presented.

2.1 Biological basics

2.1.1 Nuclear proteins

Proteins are essential for most biological processes and are involved in practically every function performed by a cell. After the sequencing of the entire genome, research turns to the study of protein function (*functional genomics*) and nuclear organization. It is of particular interest to understand how and at what specific compartment inside the nucleus gene expression is performed. It is a crucial point to determine the basic physical properties of the nuclear proteins that are involved in vital nuclear processes such as DNA replication, transcription, RNA processing and DNA repair inside the eukaryote nucleus.

The nucleus has been seen for a long time as a viscous, gel-like environment because of its high DNA content and the large amount of nuclear RNAs and proteins. With this assumption the movement of proteins within the nucleus is restricted and active transport mechanisms might be required to deliver them to their destination. This view has dramatically changed within the last years [17, 25]. The discovery and development of fluorescent markers like the Green Fluorescent Protein (GFP) combined with new in-vivo

fluorescence imaging methods have given important new insight into nuclear architecture and function. It was possible, for the first time, to determine the biophysical properties of nuclear proteins in intact cells [29]. These kinetic properties are arguably of most interest, as they underlie protein function within the cell.

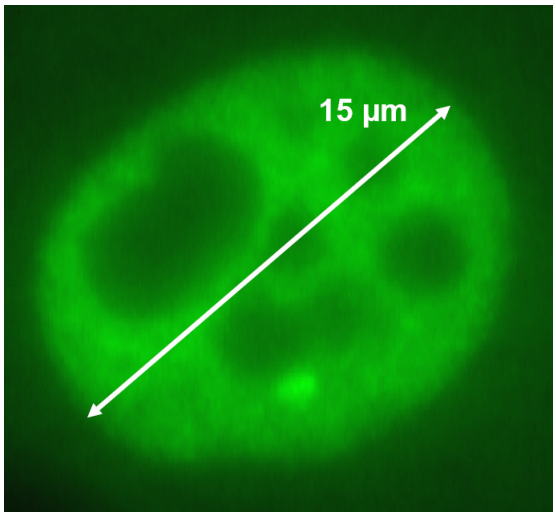

Figure 2.1: ***Glucocorticoid Receptor marked with GFP expressed in a cell nucleus****. The nucleus has a nearly elliptic shape having a long axis of* $\sim 15\,\mu m$*. The darker areas are the nucleoli which strongly differ in form and size (Picture from James McNally, NIH, Bethesda).*

Dynamic properties of nuclear proteins

A large number of nuclear proteins have now been studied with these new approaches and it has become apparent that many proteins are highly mobile within the nucleus. Their movement is independent of energy in the form of ATP and is not considerably slowed down at a lower temperature. This results constitute a diffusion based mechanism for the protein mobility. As this assumption holds for control experiments it is likely that protein movement occurs by a diffusion-based, nondirected mechanism [27, 28]. These results were obtained for many proteins, which lead to the assumption that high mobility is a general feature of nuclear proteins. Diffusion as the mean of transport is not only an energetically very economic way of movement, but ensures also the availability of the proteins throughout the nucleus. This draws a new picture of the functionality of proteins: the movement of proteins within the nucleus occurs by randomly directed diffusion. While diffusing through the nucleus the proteins frequently associate and dissociate to various binding

sites until they encounter an appropriate one. This points out that a scanning mechanism for recognizing the appropriate binding site for the proteins is needed. In [24], e.g., the dynamics of a transcription factor, namely the glucocorticoid receptor (GR), were investigated with photobleaching methods. The surprising result was that the GR molecules are continuously and rapidly exchanged. Similar observations have been made for other nuclear proteins. This stands in contrast to the traditional point of view where proteins stably bind to their binding site and remain their for a longer period during transcription.

Architecture of the nucleus

The basic architecture of the nucleus has been known for a long time. The nucleus, being the largest functional unit of a cell, varies in diameter from 10 to 20 μm. It is enclosed by a double membrane called the nuclear envelope. The inner and outer membrane fuse at regular intervals, forming nuclear pores. These pores regulate and facilitate the transport of molecules between the nucleus and the cytoplasm. Many substances are dissolved in the nucleoplasm, including proteins, and transcription factors. The genetic material (DNA) is present in the nucleus as a DNA-protein complex called chromatin. The most important functional subunit of the nucleus is the nucleolus which creates ribosomes. The ribosomes are the organelles which build a protein from a set of genetic instructions.

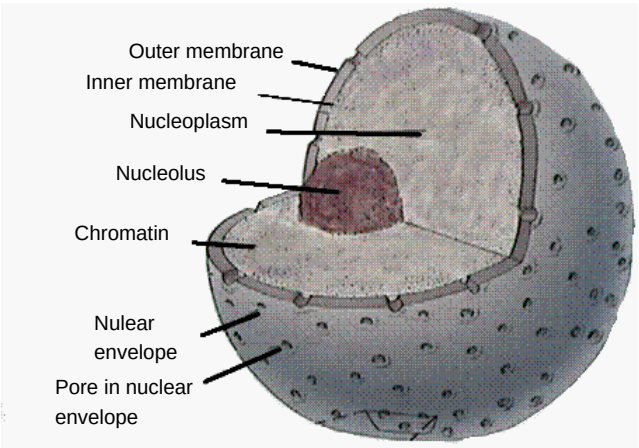

Figure 2.2: ***A typical cell nucleus****. The nuclear envelope consists of the membranes. The chromosomes as well as the nucleolus are present in the nucleus (adapted from [15]).*

The studies on protein dynamics yield new insights into the nuclear architecture and a better understanding of the nuclear functionality [14]. The nuclear

envelope restricts the flow of molecules greater than 50 kDa [8]. The various functions of the nucleus are performed in distinct compartments which are characterized by the the absence of delineating membranes. Each of them consists mainly of the proteins, which are needed for the corresponding functionality. But those proteins are not stored there until they are needed, they are continuously exchanged between the nucleoplasm and the compartment, generating steady-state structures. For most proteins the residence time in a compartment is in the order of one minute or less. The ratio of influx and efflux of proteins determines the actual morphology of a compartment. Hence, these are structures with high internal dynamics and their actual morphology represents the equilibrium situation between binding and release of nuclear proteins. These binding events actually determine how molecules move through and spatially distribute within the nucleus.

2.1.2 Green fluorescent protein

The discovery and development of fluorescent proteins as molecular tags have revolutionized our ability to study protein localization, dynamics and interaction in living cells. One of the most widely used reporter protein for FRAP experiments is the Green Fluorescent Protein (GFP).

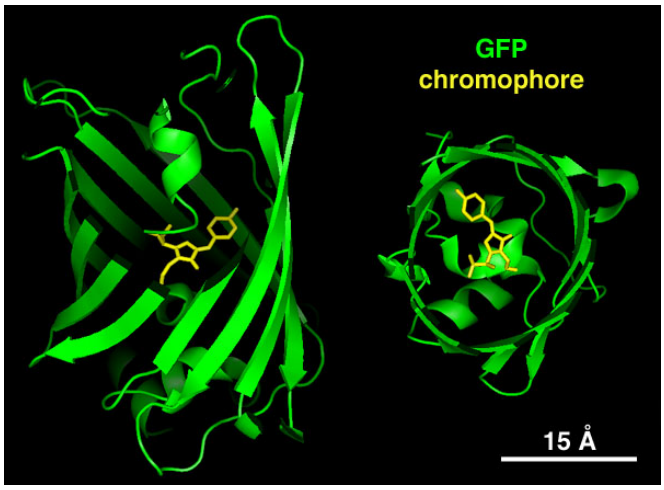

Figure 2.3: ***Chromophore location within GFP.*** *The chromophore is located on a α-helix which is inside a hollow cylinder formed by 11 β-strands (from [16]).*

GFP was first discovered as a companion protein to aequorin, the chemiluminescent protein[1] from the jellyfish *Aequora victoria*. GFP itself was found to fluoresce under excitation, requiring no jellyfish-specific enzymes, i.e., it is autofluorescent. After cloning of the gene that encodes this protein, the expression in other organisms than the jellyfish yielded a functional fluorescent protein. Therefore the gene contains all the information necessary for the synthesis of the fluorophore [34]. It has further been improved by codon optimizations which yield mutant GFPs with improved brightness, photostability and expression properties [21]. These improved characteristics are combined in a GFP variant known as enhanced GFP (EGFP). EGFP can be fused to virtually any protein using standard cloning methods. Surprisingly, the attachment of EGFP rarely affects the function and localization of the fusion protein [17]. Microscopy techniques using using GFP-tagged proteins have a number of remarkable advantages and are therefore such powerful methods for the investigation of protein properties:

- The investigation of the behavior of proteins in living cells is possible without disruption by microinjection. Hence, it is a minimally invasive tool for studying protein dynamics.
- The observations can last for long time periods because of the increased photostability.
- The imaging of the cells can be done with low light intensities, which significantly reduces the amount of harmful radiation the cell is exposed to.

GFP spectra
The wild type GFP from *Aequorea victoria* has a major excitation peak at a wavelength of 395 nm and a minor one at 475 nm. Its emission peak is at 509 nm. The major excitation peak of EGFP has been shifted to 490 nm with the peak emission kept at 509 nm (see Figure 2.4).

2.2 Experimental basics

2.2.1 Fluorescence and photobleaching

Fluorescence is an optical phenomenon in cold bodies, in which a molecule absorbs light at a particular wavelength and subsequently emits light of longer

[1] Chemiluminescence is the emission of light as the result of a chemical reaction

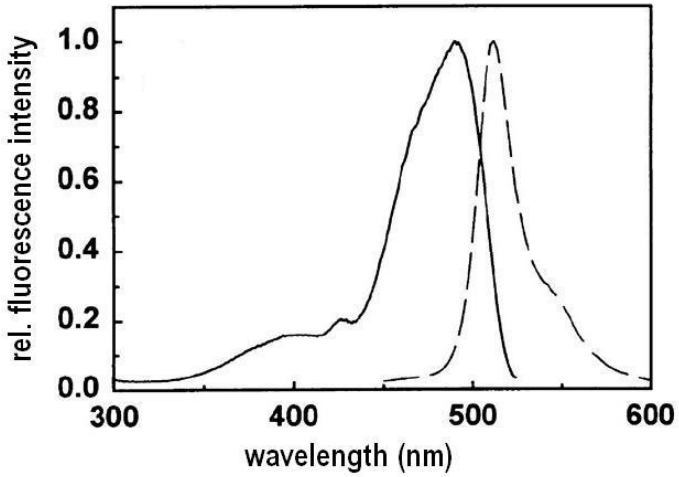

Figure 2.4: ***GFP spectra****. Excitation (solid line) and emission (dashed line) spectrum of enhanced GFP (adapted from [31]).*

wavelength after a brief interval, termed the fluorescence lifetime. The energy difference between the absorbed and emitted photons ends up as molecular vibrations [26].

Absorption-emission cycle

In the fluorescence phenomenon three major processes are involved, all of which occur on timescales that are separated by several orders of magnitude. When a fluorophore absorbs light energy, it is usually excited to a higher vibrational energy level in the first excited electronic state S_1, which happens in femtoseconds. The following rapid vibrational relaxation of the excited state to the lowest energy level occurs in about a picosecond or less. Fluorescence arises from the emission of a longer wavelength photon during relaxation to the ground state. The fluorescence lifetimes are typically four orders of magnitude slower than vibrational relaxation.

The various energy levels involved in the absorption and emission of light by a fluorophore are classically represented by a Jablonski diagram (see Figure 2.5). Here a singlet ground electronic state S_0 (lower set of parallel bars), as well as the first excited singlet state S_1 (upper set of parallel bars) is shown. At each energy level, fluorophores can exist in a number of vibrational energy levels, which are represented by the multiple lines in each electronic state. The thicker lines represent electronic states, while the thinner lines denote the various vibrational energy states. Electronic transitions are indicated with straight arrows, vibrational relaxations with wavy arrows.

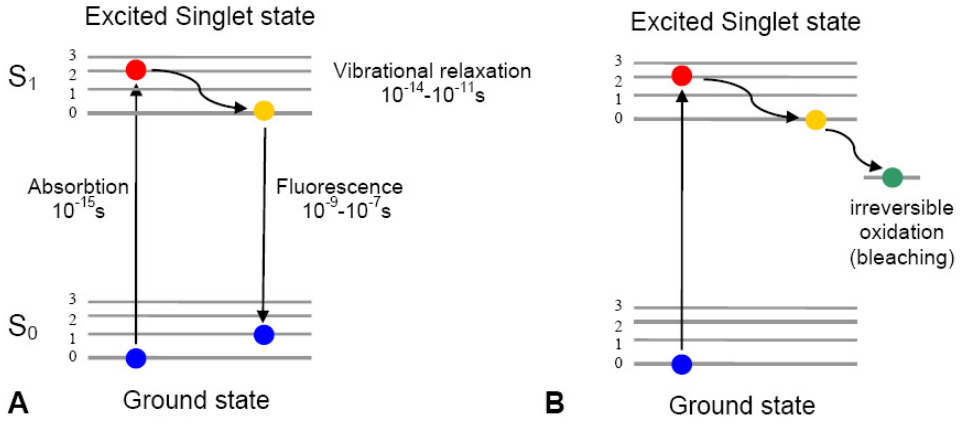

Figure 2.5: ***Jablonski diagram.*** ***A*** *The absorption-emission cycle during fluorescence process.* ***B*** *Photobleaching is assumed to be linked to a transition to the excited triplet state* T_1.

Frank-Condon principle

The different timescales during the emission-absorption cycle play a crucial role for the fluorescence process. The Frank-Condon principle states that electronic transitions take place in times that are very short compared to the time required for the nuclei to move significantly. This effect arises from the fact that the nuclei are heavier than the electrons. The excitation from the ground state to the excited state is practically an instantaneous process, so that nuclei have no time to readjust themselves during the absorption by changing the internuclear distance. Thus, the transitions are represented as vertical lines.

This is well illustrated by a potential energy diagram (Figure 2.6). The abscissa measures the distance between two nuclei of the molecule, R_0 is the equilibrium distance of the ground state. The two potential curves show the potential energy of the molecule as a function of this distance for two electronic states, a ground state and an excited state. Excitation is represented, according to the Franck-Condon principle, by a vertical arrow. In quantum mechanics each state is described by a wave function, which is identified by some quantum numbers. The quantum numbers v_0 or v_1 distinguish between the different vibrational states.

The excitation occurs from the lowest vibrational state of S_0 to a higher vibrational state of the excited singlet state S_1. The probability of the transition depends on the overlap of the wavefunctions of the initial and final state and is given by the Frank-Condon factors. This factor is calculated by the

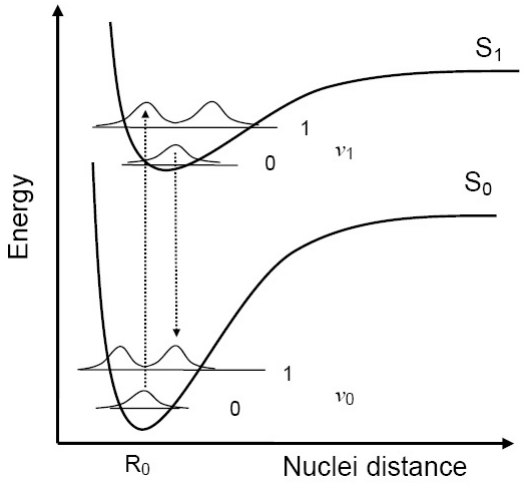

Figure 2.6: ***Frank Condon energy diagram****. This diagram illustrates the vertical electronic transition during excitation and emission of a photon.*

overlap integrals between the vibrational wave function in the ground and excited states. This means that the probability of an electronic transition depends on the degree of similarity between the wave functions describing the vibrational states of S_0 and S_1.

The molecule finds itself, after the absorption, in a nonequilibrium state and begins to vibrate. The excited state has a sufficiently long lifetime, so that the molecules can achieve a thermally equilibrated lowest-energy excited state by converting the excess vibrational energy to heat and exchanging it with the environment. The fluorescence emission of the photon will therefore in general occur from the lowest excited singlet state (a behavior known as Kasha's rule). Thus the energy of the emitted photon will be less than that of the exciting photon and the wavelength is shifted to longer values. This phenomenon is generally known as Stokes Shift.

Photobleaching

Photobleaching occurs when a fluorophore permanently loses the ability to fluoresce. Each fluorophore has different photobleaching-characteristics. Its stability can be characterized by the average number of absorption-emission cycles that the molecules of this fluorophore undergo before they are irreversibly photobleached. The number of cycles depends on the local environment and the molecular structure and is, therefore, a fluorophore-specific property. The exact mechanism of photobleaching is yet not known, but it is assumed to be linked to a transition from the excited singlet state S_1 to the

excited triplet state T_1 (see Figure 2.5B), a process called intersystem crossing. This transition withdraws the molecule from the absorption-emission cycle and as the triplet state is relatively long-lived with respect to the singlet state it is chemically more reactive. Thus excited molecules have a much longer timeframe to undergo further chemical reactions with components in the environment that are the basis for bleaching reactions [13].

2.2.2 Confocal laser scanning microscope

The development of confocal laser scanning microscopes (CLSM), in conjunction with GFP as molecular tag, provided scientists with an excellent standard tool to perform FRAP experiments. This section covers only the most important topics for understanding the functionality of a CLSM. A thorough explanation can be found in [26].

Widefield optical epi-fluorescence microscope
In traditional *widefield* fluorescence microscopy, the entire specimen is subjected to intense light from an illumination source, usually a mercury lamp. The resulting image of secondary fluorescence emission can be viewed directly in the eyepieces or be detected by a camera (usually a CCD camera). In an *epi* configuration, the illumination source is placed on the same side of the specimen as the objective, which then serves as both the condenser and the imaging lens system. Optical filters are used to separate excitation light from emission light:

- The **excitation filter** permits only selected excitation wavelengths to pass through on the way toward the specimen.
- **Barrier filters** are designed to absorb the excitation wavelengths and permit only selected emission wavelengths to pass toward the eye or other detector.
- **Dichromatic beamsplitters** are specialized filters which are designed to efficiently reflect excitation wavelengths and pass emission wavelengths.

The major disadvantage of these microscopes is that the excitation occurs through the whole volume and is not restricted to the plane of focus. Therefore emitted fluorescence from above and below the plane of focus (out-of-focus light) obscures resolution of features that lie in the objective focal plane.

Confocal laser scanning microscope

The light source of a laser scanning microscope is one or more laser(s). The use of a laser as illumination source has two major consequences. First, the excitation light bandwidth is determined by the source and not by an excitation filter and thus is much narrower than in fluorescence microscopy (2-3 nm rather than 20 - 30 nm). Second, in order to illuminate the whole visual field, the laser beam has to scan the sample sequentially point by point and line by line. The fluorescence detected at each point is measured in a photomultiplier tube (PMT) and the image is built up by assembling all the pixel information to one image. This method of illumination has enormous advantages in that it is possible to illuminate selected regions of the visual field.

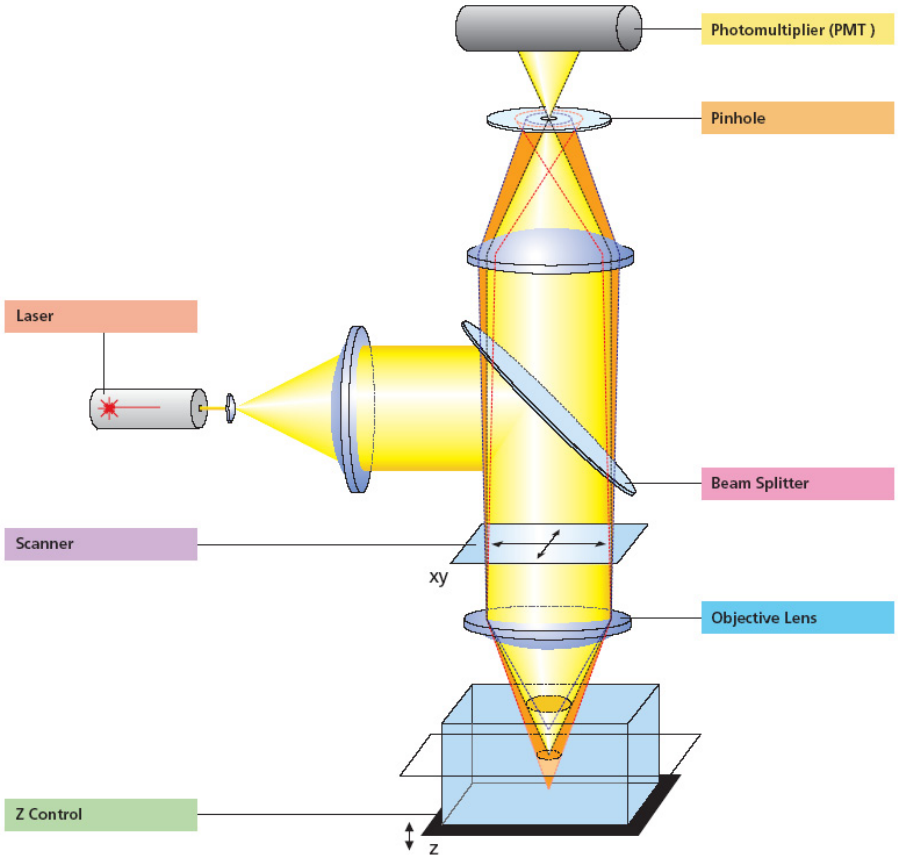

Figure 2.7: ***Principle of a confocal laser scanning microscope****. The illumination is performed with a laser beam, which scans the the whole visual field. A pinhole reduces the out of focus light (from [26]).*

The basic key to the confocal approach is the use of a spatial filtering technique to eliminate the out-of-focus light in specimens whose thickness exceeds the immediate plane of focus. A pinhole sitting conjugated to the focal plane (i.e., confocal) keeps light from the PMT that is emitted from others than the focal plane. This means that the only light to enter the PMT, and thus detected, comes from near the focal plane of the objective lens. Thus, a CLSM can image optical slices of the specimen can be imaged with high contrast and high resolution in x, y and z. By moving the focus plane in z-direction single images (optical slices) from the focal plane can be recorded. This slides can be digitally processed and put together to reconstruct an image of the 3-dimensional object.

Acoustic-optic tunable filter
The acoustic-optic tunable filter (AOTF) is an electro-optic device that allows the modulation of the intensity of the illumination laser light. A confocal laser-scanning microscope equipped with an AOTF enables the user to vary the intensity of illumination on a pixel by pixel basis. Acting in this manner, an arbitrary geometry for the scanned region can be defined and be illuminated more intensely. This feature makes such microscopes suitable for FRAP experiments. The user can define an arbitrary bleach pattern in the sample, the AOTF switches the laser power during bleaching rapidly between the high intensity bleaching inside the bleach spot and negligible intensity outside. In addition, the AOTF controls the intensity for the subsequent imaging.

Point spread function
Geometrical optics predicts that theoretically the image of a point source of light produced by an image-forming optical system is a point. But the image of a point produced by a real optical system is not a point but a small, blurred spot, which is known as Airy disk. In real space the system response is not only in the lateral direction, i.e., the Airy disc, but it extends to all three dimensions. The resulting three-dimensional intensity distribution of a points source is called the point spread function (PSF) or the impulse response of the optical system.

An extended object can be considered as a superposition of an infinite number of points sources and each of these points is blurred individually by the PSF. Therefore, each point in the object contributes to each point in the image. The resulting image is formed from the contributions of each blurred spot images. The image intensity $I(x, y)$ can be calculated with the convolution of the object intensity $O(x, y)$ and the point spread function $PSF(x, y)$ of the system:

$$\begin{aligned} I(x,y) &= PSF(x,y) \otimes O(x,y) \\ &= \int_{-\infty}^{\infty}\int_{-\infty}^{\infty} PSF(x-x',y-y')\,O(x',y')\,dx'\,dy'. \end{aligned} \tag{2.1}$$

The ideal case would be a system that produces an image which is identical to the object. This behavior can be mathematically be described by PSF's consisting of delta functions for each independent variable:

$$PSF(x,y) = \delta(x)\,\delta(y). \tag{2.2}$$

By using this PSF for Eq. 2.1, the object intensity is directly mapped to the image intensity.

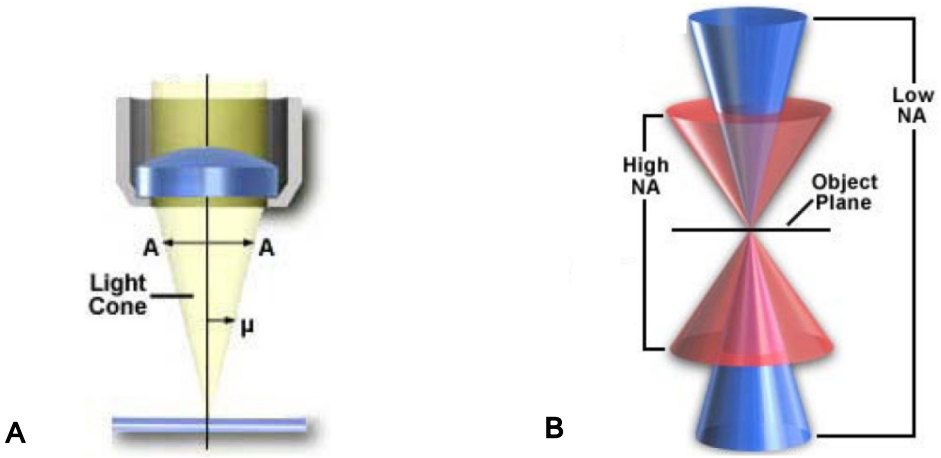

Figure 2.8: ***Numerical aperture (NA).*** ***A*** *The NA depends on the half angle μ of the light cone collected by the objective.* ***B*** *Objectives with a high NA collect more light and yield a better resolution. (from [26]).*

Numerical aperture and resolution

The image in a light microscope is formed by light waves which are emitted by the specimen and enter the objective in an inverted cone. The numerical aperture (NA) is a measure of its ability to collect this light. It can be calculated with the the half angle μ of the cone of light collected by the objective lens and the refractive index n of the medium between the specimen and the lens:

$$NA = n \sin(\mu). \tag{2.3}$$

The *resolution* of a microscope is defined as the smallest distance between two points that can still be distinguished as two separate entities. It is determined by the numerical aperture and the wavelength of light used for imaging. The well-known Rayleigh criterion for lateral resolution is based on the fact that the image of a point source is an Airy disk. It states that two points can be resolved if the distance between them is larger than the radius of the corresponding Airy disc. The radius of such a disc observed in a CLSM , i.e., the resolution, can be calculated with the following equation:

$$R_{lateral} = \frac{0.4\,\lambda}{NA}, \tag{2.4}$$

where $R_{lateral}$ is the resolution in the image plane, λ is the emission wavelength, NA is the numerical aperture [26].

There are various formulae for the calculation of the *axial resolution*. One equation commonly used to describe axial resolution for the confocal configuration is:

$$R_{axial} = \frac{1.4\,n}{NA^2}, \tag{2.5}$$

where R_{axial} is the axial resolution, the other variables are specified as previously.

Illumination intensity profile

As mentioned above, the objective in a CLSM has as double role and serves as condenser, too. The laser beam is first expanded and then focused by the objective lens system to a very small spot in the focal plane (Figure 2.7). This spot is not infinitely small, but has a finite volume. The actual intensity profile of the laser can be taken to be Gaussian in the axial as well as the radial direction:

$$I(r,z) = I_0\, e^{-2\left(\frac{r^2}{w^2}+\frac{z^2}{z_0^2}\right)}, \tag{2.6}$$

where w and z_0 are the radii of the laser beam intensity in the radial and axial directions where the intensity decreased to $e^{-2} \approx 0.13$ of its maximum value I_0 [4, 6]. The numerical aperture determines not only the radial and axial resolution, but also the radii of the laser beam intensity profile. Thus, they have an analogous functional dependency on the numerical aperture. A small numerical aperture yields therefore a large value for z_o. It is common practice for FRAP experiments to consider lenses of relatively low NA to have an almost cylindrical illumination profile [5].

2.2.3 Qualitative FRAP

Biomolecules that are tagged with a fluorescent dye, can be measured with respect to both position and concentration using fluorescence microscopy. Under typical experimental conditions, the rapid exchange of proteins between the nucleoplasm and their nuclear compartments yields the dynamic steady-state as described in section 2.1.1. The concentrations of the fluorescent proteins are hence in equilibrium. In addition, these molecules are too abundant to resolve the movement of individual proteins. This enables only the tracking of the steady-state compartments by direct fluorescent visualization but it is not possible to directly reveal the movement of single proteins [22, 29].

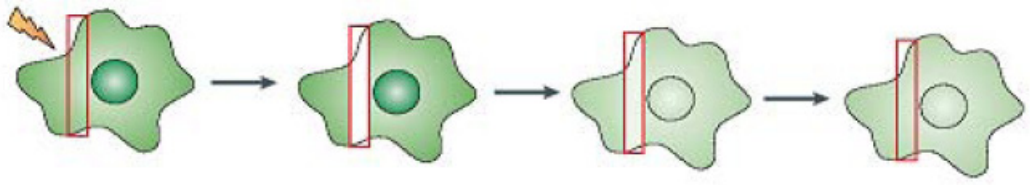

Figure 2.9: ***Fluorescence recovery after photobleaching****. The fluorescence intensity is measured in a small area after bleaching by a short laser pulse. (adapted from [20]).*

Fluorescence recovery after photobleaching (FRAP) is a method that makes the measurement of molecular dynamics possible. This is done by introducing a rapid shift away from the steady-state distribution without disrupting the actual concentration of the molecule under study. FRAP makes just one fraction of the fluorescent proteins invisible. This is achieved by irreversibly photobleaching of fluorescent molecules in a small area of the cell by a high-powered focused laser beam. This creates condition where the molecules outside the photobleached region are fluorescent, whereas the molecules within the photobleached region are nonfluorescent. The fluorescent and nonfluorescent proteins will mix over time until a steady-state distribution of the photobleached and fluorescent copies of the protein is achieved. The subsequent movement of the non-bleached fluorescent molecules into the bleached area leads to a recovery of fluorescence, which is recorded at low laser power. The proteins interact with many partners *in vivo* and these interactions determine their apparent mobility. Hence, the FRAP recovery kinetics reflect the dynamic properties of the protein of interest and careful interpretation of the data yields much qualitative information on the mobility of a protein [29].

Fluorophores for FRAP
The fluorophores that are used as fluorescent markers should in general not inhibit the function of the investigated molecule. For FRAP experiments there are two additional demands concerning the photostability. First, the fluorophore should be bright and stable under low intensity illumination, which is important during image acquisition in the pre- and postbleach phase. Second, the fluorophores should bleach fast and irreversibly under high intensity illumination during the bleach phase.

2.2.4 FRAP with a CLSM

FRAP experiments can be performed on a standard commercially available confocal laser-scanning microscope equipped with an acousto-optical tunable filter. The user can interactively define an arbitrary bleach region of interest (ROI). After the definition of the bleach pattern, the microscope scans the laser beam over the sample and increases the intensity inside the ROI significantly to perform the photobleaching [5]. Figure 2.10 shows a schematic representation of the bleaching process. The laser beam has as certain width (indicated by the smaller gray circle) and is scanned at a defined speed v line by line over the sample. To bleach the defined circular spot with a radius w_b the scanning of n lines is necessary. The intensity is controlled by the AOTF and is set to a high value inside the user defined region (thick lines) and nearly to zero outside (dashed lines). For imaging, the monitoring beam scans the whole sample with constant illumination intensity. The resulting image contains the bleached ROI and consists of N scanned lines. The fluorescence intensity is extracted from a set of pixels inside a circle with radius w_s (usually $w_s = w_b$) with an image processing tool.

Impact of the numerical aperture (NA)
Depending on the required resolution and the desired depth of bleaching, different objectives are suitable for FRAP experiments. For homogeneous bleaching in z-direction objectives with a lower numerical aperture (like 0.7) lens are suitable, but this will result in a lower resolution. By using objectives with a high numerical aperture (like 1.4), increased light intensity in the focal plane but incomplete bleaching in z-direction can be achieved. In general can be said that the thinner the structure subjected to bleaching the higher the NA should be.

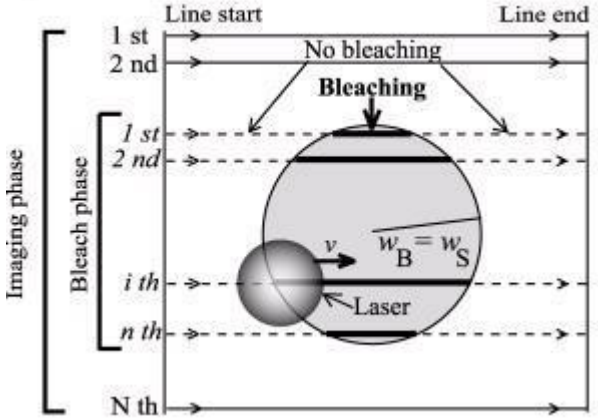

Figure 2.10: ***Bleaching with a CLSM****. The laser beam which scans the sample at speed v is indicated by the gray circle. Within the bleach pattern the laser intensity is increased by the AOTF to perform the photobleaching (thick line). (from [6]).*

2.2.5 Quantitative FRAP

The measured data from a FRAP experiment is the time-dependent recovery of the fluorescence intensity inside the bleach spot, the so called **FRAP recovery curve**.

Normalization
An important step to accurately quantify the results of an experiment is the normalization of the experimental data [9]. The data must be corrected to account for changes in the total fluorescence intensity throughout the course of the experiment. During the initial photobleaching process, a significant fraction of the fluorescent protein is made non-fluorescent. This reduces the theoretical maximum intensity that the photobleached region may recover to from its initial intensity after bleaching. In addition is the cell exposed to many iterations of laser illumination during the collection of the data for the recovery curve. This may also result in some photobleaching. In FRAP experiments, typically $\sim$ 10% of fluorescence is lost during the bleaching process and less than 5% is lost during the imaging phase [6].

Phair and Misteli introduce a normalization method which is widely used for FRAP experiments [28]. The fluorescence signal measured in a region of interest is normalized to the change in total fluorescence as follows:

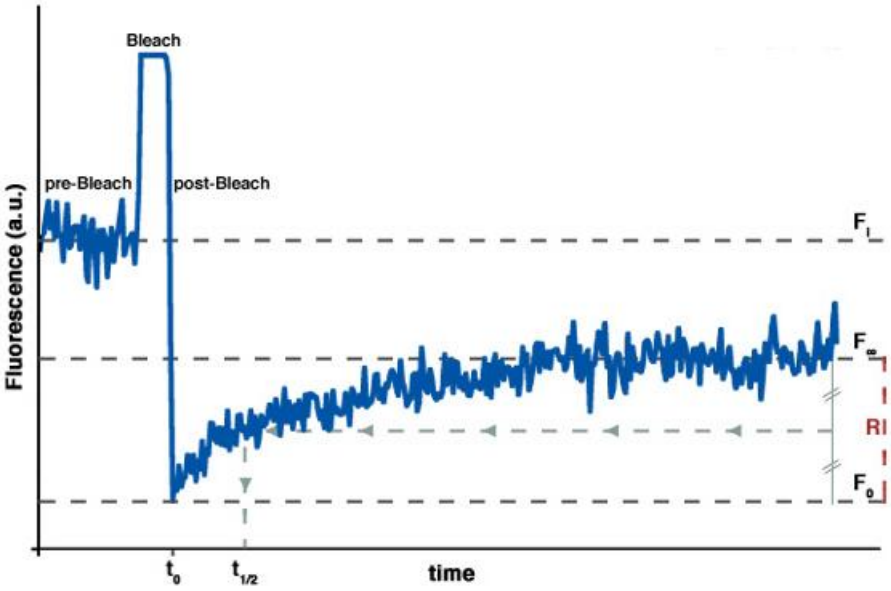

Figure 2.11: ***FRAP recovery curve****. The fluorescence intensity in a region of interest is plotted versus time. The prebleach value F_I compared with the asymptote of the recovery F_∞ can be used to calculate the mobile fraction. The diffusion time $\tau_{1/2}$ holds information about the mobility of the protein (from [16]).*

$$F(t) = \frac{I(t)\, T_0}{I_0\, T(t)}, \tag{2.7}$$

where T_0 is the total fluorescence intensity in the nucleus and I_0 the intensity of the bleached region before bleaching. $T(t)$ and $I(t)$ are the fluorescence intensities at time t in the nucleus and the bleached region, respectively.

Measurable biophysical properties

Depending on the complexity of the interaction of the protein of interest, the curve may have different shape. Until recently only two parameters could be deduced from FRAP experiments: the mobile fraction of fluorescent molecules and the diffusion coefficient [30].

The **mobile fraction**, which is the fraction of fluorescent proteins that can diffuse into the bleached region during the time course of the experiment, can be calculated from

$$R = \frac{F_\infty - F_0}{F_I - F_0}, \tag{2.8}$$

where F_∞ is the fluorescence in the bleached region after full recovery, F_I is the fluorescence before bleaching and F_0 is the fluorescence just after the bleach.

When protein motion is due to diffusion, the mobility can be expressed by the **diffusion coefficient** D, see section 2.3.1 for details. The diffusion coefficient can be calculated from the characteristic diffusion time $\tau_{1/2}$. The diffusion time is the time necessary for the fluorescence to recover half between the fluorescence level after photobleaching (F_0) and the fluorescence at the plateau level (F_∞). Most formulas describing this relationship are based on a model worked out by Axelrod [3]. This model is valid for circular bleach spots generated by a stationary Gaussian laser beam and assumes two-dimensional diffusion. The diffusion coefficient can be calculated by

$$D = \frac{\omega^2}{4\,\tau_{1/2}}, \tag{2.9}$$

where ω is the half width of the laser beam intensity at e^{-2} height.

Kinetic modeling
It is virtually impossible to measure pure diffusion of a protein in living cells since its mobility is influenced by the interactions with many partners [29]. The measured FRAP curve therefore contains not only information about the diffusion of a protein, but also about its binding affinity. Modern kinetic modeling approaches consider this fact and describe a hypothesized biological system with a mathematical model. This model depends on the biophysical parameters of the protein, such as diffusion coefficient and binding rates [9, 29, 32]. Data fitting routines enable the estimation the set of parameters that result in the best agreement with the experimental data. Acting in this manner, the mathematical model can be tested and quantitative information about its parameters can be obtained.

2.3 Mathematical model

The dynamic behavior of nuclear proteins in living cells is described detailed in section 2.1.1. Proteins diffuse through the nucleus and undergo reversible binding-unbinding processes with nuclear structures. This structures are assumed to be immobile on the time scale of the FRAP experiment and spatially homogeneously distributed. In this section this biological model is translated into a mathematical description (*kinetic modeling*). The resulting model consists of a system of reaction-diffusion equations, i.e., a system of partial differential equations, which has been applied in the context of reversible chemical reactions [12].

2.3.1 Diffusion - the mean of transport for proteins

Diffusion is the physical process by which matter is transported from regions of high concentration to regions of lower concentration. This is the macroscopic result of the random thermal motion also known as Brownian motion on a microscopic scale.

Diffusion equation
The mathematical theory of diffusion is based on the hypothesis that the transfered rate of mass is proportional to the concentration gradient. Fick (1855) stated that the flux of mass in one dimension due to diffusion is proportional to the spatial gradient of the corresponding solute concentration [1]. This law can be applied for each spatial variable independently. The flux of mass in three dimensions, described by the vector $\vec{J}$ ($mol\,m^{-2}\,s^{-1}$), can thus be calculated with the spatial gradient of the solute concentration c ($mol\,m^{-3}$) according to the following formula:

$$\vec{J} = -D\left(\vec{e}_x\frac{\partial c}{\partial x} + \vec{e}_y\frac{\partial c}{\partial y} + \vec{e}_z\frac{\partial c}{\partial z}\right) = -D\,\nabla c. \tag{2.10}$$

The constant of proportionality is the diffusion coefficient D ($m^2\,s^{-1}$). The negative sign reflects the fact that $\vec{J}$ is directed from higher to lower concentrations.

From vector analysis is known that the divergence of a vector field $\vec{J}$, which describes the flux of a quantity, is related to the time dependent change of this quantity within an infinite volume element. Since $\vec{J}$ in Eq. 2.10 describes the flux of mass M (mol) during a diffusion process, the divergence of $\vec{J}$ describes the change of mass with respect to time. This change can also be expressed by the the local change in the solute concentration:

$$\frac{\partial M}{\partial t} = -\nabla\,\vec{J}\,dV \quad \text{with } \frac{\partial M}{\partial t} = \frac{\partial c}{\partial t}\,dV \;\Rightarrow\; \frac{\partial c}{\partial t} = -\nabla\,\vec{J}. \tag{2.11}$$

The flux of mass $\vec{J}$ can be expressed with Eq. 2.10 yielding *Fick's 2nd law*. It describes the time-dependent diffusion of a substance with molar concentration c:

$$\frac{\partial c}{\partial t} = -\nabla\vec{J} = D(\frac{\partial^2 c}{\partial x^2} + \frac{\partial^2 c}{\partial y^2} + \frac{\partial^2 c}{\partial z^2}) = D\,\nabla^2 c. \tag{2.12}$$

It states that the time rate of concentration change is related to the second derivative with respect to each space variable expressed by the Laplacian operator ∇^2.

Diffusion coefficient for biomolecules
The diffusion coefficient D is a constant that describes how fast or slow an object diffuses through a fluid. It depends on both the size and shape of the particle, and the viscosity and temperature of the fluid. The diffusion coefficient D for globular particles can be calculated with the Stokes-Einstein Equation [23]:

$$D = \frac{kT}{6\pi\eta R_h}, \tag{2.13}$$

where T is the absolute temperature, η the viscosity of the solution, k the Boltzmann constant, and R_h the hydrodynamic radius of the particle. For FRAP experiments the absolute temperature is usually constant within the cell and thus the most important factors underlying D are the size of a protein and the viscosity of the medium. Table 2.1 provides typical values of the diffusion coefficient for GFP and a GFP chimera[2] that illustrate the marked differences:

Table 2.1: Diffusion rates of GFP and GFP chimera using FRAP [22, 32].

Molecule	$D(\mu m^2 s^{-1})$
GFP in water	87
GFP in cytoplasm	25
GFP tagged glucocorticoid receptor in cytoplasm	9.2

The first two values are diffusion coefficients of GFP in different environments. In cytoplasm the mobility of proteins is significantly reduced compared to water. This is expressed by a larger value for the viscosity η and according to Eq. 2.13 by a smaller value for D. The attaching of GFP as fluorescent marker to the glucocorticoid receptor results in a protein with increased molecular weight M. As an approximation this chimera can still be regarded to be globular, so the proportionality $D \propto R^{-1} \propto M^{-1/3}$ is still valid. The attaching of GFP yields a larger protein with a decreased value for the diffusion coefficient.

Diffusion describes the recovery process
During FRAP experiments a fraction of the fluorescent labeled molecules is made invisible. After the bleaching two pools of the same protein exist: one with the fluorescent proteins and one with the bleached proteins. Acting in

[2]In genetics, a chimera is a hybrid protein

this manner, FRAP alters the fluorescent steady state in a cell but without introducing a gradient for of total protein concentration. For both pools exists a concentration gradient after the bleaching and their dynamics can be described with Eq. 2.12 independently of each other. The fluorescence intensity recovery is governed by the dynamics of the fluorescent pools, thus only those proteins have to be considered.

Two-dimensional diffusion
In many theoretical FRAP analyses the diffusion of the proteins is assumed to be two-dimensional in the focal plane [32]. This assumption is valid if either thin samples or low numerical aperture (NA) optics for thick samples are used. In thin samples the mobility of the proteins is restricted by the geometry itself to two dimensions. For thick samples the bleaching can be performed with objectives with a low NA. A laser beam which is created with a conventional confocal laser scanning microscopes with low NA optics has an essentially cylindrical intensity profile (see section 2.2.2). Thus, the same amount of photobleaching is generated in each lateral plane along the optical axis if absorption losses along this axis are neglected [7]. In this case, axial terms disappear from the Laplacian (∇^2) in Eq. 2.12 and only the radial components remains. The recovery in the bleached area will mainly arise from diffusion off non bleached fluorescent molecules in the focal plane.

2.3.2 Reaction kinetics

A protein that undergoes a single binding reaction can be described by a second order reversible reaction:

$$F + S \underset{k_{off}}{\overset{k_{on}}{\rightleftarrows}} C, \tag{2.14}$$

where F represents free proteins, S represents vacant binding sites, C represents bound FS complexes. The binding rates k_{on} and k_{off} describe the binding affinity of the protein. In addition, the binding rates hold information about residence times. The average time for diffusion to the next site is given by $\tau_d = 1/k_{on}$ and the average binding time per site is given by $\tau_b = 1/k_{off}$ [32]. For example, a large value for k_{off} corresponds to a protein that releases quickly after binding, i.e., it is weak bound to its binding site. Whereas a large value for k_{on} describes the situation of a free protein with a very short diffusion time, i.e., is immediately involved in a bound complex. The interaction of proteins with its partners can be formulated mathematically with rate laws, which describe the time progress of the reaction:

$$\begin{aligned} \frac{\partial f}{\partial t} &= -k_{on} f s + k_{off} c \\ \frac{\partial s}{\partial t} &= -k_{on} f s + k_{off} c \\ \frac{\partial c}{\partial t} &= +k_{on} f s - k_{off} c, \end{aligned} \tag{2.15}$$

in which the molar concentration of a participant J is given by $[J] = j$.

2.3.3 One-binding-state model

This model describes proteins that bind reversibly to one specific binding site. The equations that describe the protein dynamics must incorporate diffusion as the mean of transport (Eq. 2.12) and the rate laws to describe the binding reaction (Eq. 2.15). The most general case is a set of three coupled reaction-diffusion equations:

$$\begin{aligned} \frac{\partial f}{\partial t} &= D_f \nabla^2 f - k_{on} f s + k_{off} c \\ \frac{\partial s}{\partial t} &= D_s \nabla^2 s - k_{on} f s + k_{off} c \\ \frac{\partial c}{\partial t} &= D_c \nabla^2 c + k_{on} f s - k_{off} c. \end{aligned} \tag{2.16}$$

Simplification
These equations can be simplified considerably by two assumptions that are valid for many biological situations [8, 32]:

1. The subcellular structures, to which the fluorescent proteins bind, is assumed to be spatially homogeneous distributed and immobile at least on the time- and length-scale of the FRAP measurement. Ignoring diffusion of the bound complex and vacant binding site results in $D_c = 0, D_s = 0$ in the second and third equation of Eq. 2.16.

2. The photobleaching is performed on a equilibrated biological system expressed by a uniform steady-state distribution of the concentrations. In addition there is conservation of mass during the FRAP experiment, i.e., there is no net growth of the fluorescent population. This is reasonable since most FRAP experiments occur on a timescale of seconds to several minutes, whereas GFP fusion proteins expression changes over

a time course of hours. The corresponding equilibrium concentrations of F, S, and C are denoted by F_{eq}, S_{eq} and C_{eq}. Although bleaching changes the number of visible free and bound molecules (F and C), it does not change the number of free binding sites. Therefore s can be considered as a constant throughout the photobleaching recovery. This eliminates the second equation in Eq. 2.16. In the remaining equations the term $k_{on}\, s = k_{on}\, S_{eq}$ is replaced by the so called pseudo-on rate k^*_{on}.

With these two assumptions, the expressions in Eq. 2.16 reduce to

$$\begin{aligned} \frac{\partial f}{\partial t} &= D_f\, \nabla^2 f - k^*_{on} f + k_{off} c \\ \frac{\partial c}{\partial t} &= k^*_{on} f - k_{off} c. \end{aligned} \tag{2.17}$$

Equilibrium concentrations
The equilibrium concentrations of the free and bound proteins during the pre-bleach phase are F_{eq} and C_{eq}. The system is at equilibrium if there are no changes of the concentrations with respect to time. Thus, the derivatives with respect to time in 2.17 must be zero. The Laplacian $\nabla^2 F_{eq}$ will be zero if there is no concentration gradient, which is true for the equilibrated system. With these conditions F_{eq} and C_{eq} can be calculated with the ratio of the binding rates:

$$\frac{\partial f}{\partial t} = \frac{\partial c}{\partial t} = 0 \;\Rightarrow\; k^*_{on}\, F_{eq} = k_{off}\, C_{eq} \;\Rightarrow\; C_{eq} = F_{eq} \frac{k^*_{on}}{k_{off}} \tag{2.18}$$

2.3.4 Two-binding-state model

In this model a second independent binding state is present and the chemical rate equations become

$$F + S_1 \underset{k_{1off}}{\overset{k_{1on}}{\rightleftarrows}} C_1, \qquad F + S_2 \underset{k_{2off}}{\overset{k_{2on}}{\rightleftarrows}} C_2, \tag{2.19}$$

where subscripts 1 and 2 refer to the different binding states. With the same assumptions that led to Eq. 2.17 for the one-state model, reaction-diffusion equations for the two-binding-state model can be derived:

$$\begin{aligned}
\frac{\partial f}{\partial t} &= D_f \nabla^2 f - k^*_{1on} f + k_{1off} c_1 - k^*_{2on} f + k_{2off} c_2 \\
\frac{\partial c_1}{\partial t} &= k^*_{1on} f - k_{1off} c_1 \\
\frac{\partial c_2}{\partial t} &= k^*_{2on} f - k_{2off} c_2. \qquad (2.20)
\end{aligned}$$

The equilibrium concentrations F_{eq}, C_{1eq}, and C_{2eq} can be calculated with the same considerations as for the one-binding-state model:

$$\frac{\partial f}{\partial t} = \frac{\partial c_1}{\partial t} = \frac{\partial c_2}{\partial t} = 0 \;\Rightarrow\; C_{1eq} = F_{eq} \frac{k^*_{1on}}{k_{1off}} \;\;,\;\; C_{2eq} = F_{eq} \frac{k^*_{2on}}{k_{2off}}. \qquad (2.21)$$

2.3.5 Boundary conditions

The protein dynamics can be described in terms of a system of partial differential equations, more precisely by parabolic partial differential equations. The initial values for this system are defined by the photobleaching process. The boundary conditions can be derived from biological considerations. The nuclear membrane is a common diffusional barrier, which separates the nucleus from the cytoplasm. During the time scale of the experiment there is no flux of fluorescent biomolecules into or out of the nucleus. The negligible flux through the nuclear membrane can be described mathematically by no-flux Neumann boundary conditions at the membrane Γ:

$$\vec{n} \nabla f \Big|_{\Gamma} = 0, \qquad (2.22)$$

where $\vec{n} \nabla f$ the normal derivative of the concentration f at the boundary. With this additional assumption the model becomes an initial-value problem subject to Neumann(no-flux) boundary conditions [10].

2.3.6 Recovery curve

The solution of Eq. 2.17 or 2.20, either obtained by an analytical or numerical approach, yields the time dependent values of the concentrations of the free and bound proteins. This is, however, not the fluorescence intensity recovery curve which is obtained from a real FRAP experiment. In order to compare the results from a simulation to the result from an experiment it is necessary to transform the calculated distribution of the fluorophore to a fluorescence intensity image as seen by the microscope [5]. A very important prerequisite is the existence of a space independent relation between the

concentration of fluorescent molecules and the fluorescence intensity. Due to this proportionality the protein concentration can be used to calculate the fluorescence intensity within the bleach spot.

Early applications of FRAP used nonscanning microscopes. Bleaching and image acquisition was performed with a stationary laser beam at the bleach spot. For such cases the total FRAP intensity $F(t)$ at time $t \geq 0$ can be calculated with the integral [3]:

$$F(t) = q \iint_{\Omega} I_d(x, y) \cdot (f(x, y, t) + c(x, y, t)) \; dx \; dy \tag{2.23}$$

over the bleach spot Ω. The constant factor q takes all relevant factors concerning illumination and light collection into account, $I_d(x, y)$ is the laser intensity during detection, $f(x, y, t)$ and $c(x, y, t)$ are the concentrations of the free and bound proteins, respectively.

Currently, FRAP experiments are performed on confocal laser scanning microscopes, where bleaching and monitoring of fluorescence are done in a fundamentally different way. In such systems a laser beam scans the sample sequentially point by point. The image formation can mathematically be described by the convolution of each point in the sample with the point spread function (PSF) of the microscope (see section 2.2.2). The fluorescence intensity recovery can afterwards be extracted from this image. Fortunately, this process can be simplified if the experimental conditions meet certain assumptions [5]. Among the most important are that the radial resolution of the detecting laser beam is much smaller than the scanned structure, and that objectives of low numerical aperture are used. In this case the total fluorescence within the bleach spot can be calculated with Eq. 2.23 as if the detecting laser beam is stationary at the bleach spot position and has an uniform intensity distribution.

2.3.7 Analytic solution

Sprague et al. derive an analytical solution for the FRAP recovery within a circular bleach spot [32]. They introduce an additional assumption: the size of the bleach spot must be small relative to the size of the fluorescent department. The nucleus can now be considered to be infinite sized. This has two major consequences:

- The fluorescence intensity recovers to the initial pre-bleach value. Without this assumption some measurable fraction of fluorescence will be lost during the bleaching.

- The infinite-sized nucleus yields the boundary condition $c(r \pm \infty, t) = C_{eq}$ for all times t. The analytical solution is calculated by the application of the Laplace transformation. The above boundary conditions are essential for the applicability of this method.

The circular bleach spot together with the infinite nucleus allows a description of the geometry in terms of composite cylindrical regions. The space dependency can be described by a single variable, namely the radius r.

The one and two-binding-state model are solved by analogy with a heat conduction problem described in [11]. In order to follow this approach the variables that describe the concentrations are transformed: immidately after the bleaching they are zero outside the bleach spot and inside they have their equilibrated values. The reaction-diffusion equations of the transformed variables can be Laplace transformed which yield a new set of differential equations (modified Bessel equations). The solution for this equations can be expressed in terms of Bessel functions, which describe the free and bound fluorescence intensity in the Laplace domain. The integration of this values over the bleach spot results finally in the Laplace transformation of the FRAP recovery curve, the inversion yields the time-dependent FRAP recovery.

One-binding-state model
Acting in this way Sprague et al. show that for a single binding reaction the average of the Laplace transform of the fluorescence intensity within the bleach spot is given by

$$\begin{aligned} \overline{frap}(p) \quad &= \quad \frac{1}{p} - \frac{F_{eq}}{p}(1 - 2\,K_1(q\,w)I_1(q\,w)) \\ &\quad \times \left(1 + \frac{k^*_{on}}{p + k_{off}}\right) - \frac{C_{eq}}{p + k_{off}}, \\ &\text{where} \quad q^2 = \left(\frac{p}{D_f}\right)\left(1 + \frac{k^*_{on}}{p + k_{off}}\right), \end{aligned} \tag{2.24}$$

where w is the radius of the bleach spot, D_f the diffusion coefficient, I_1 and K_1 are modified Bessel functions of the first and second kind, F_{eq} and C_{eq} are the equilibrium concentrations (see Eq. 2.26), p is the Laplace variable. The inverse transformation of Eq. 2.24 can be computed numerically to yield the predicted FRAP recovery curve as function of time.

Two-binding-state model
For two binding reactions the Laplace transform of the fluorescence intensity can be calculated with the following formula:

$$\begin{aligned}\overline{frap}(p) &= \frac{1}{p} - \frac{F_{eq}}{p}(1 - 2\,K_1(q\,w)I_1(q\,w)) \\ &\quad \times \left(1 + \frac{k^*_{1on}}{p + k_{1off}} + \frac{k^*_{2on}}{p + k_{2off}}\right) - \frac{C_{1eq}}{p + k_{1off}}\frac{C_{2eq}}{p + k_{2off}}, \\ \text{where} \quad q^2 &= \left(\frac{p}{D_f}\right)\left(1 + \frac{k^*_{1on}}{p + k_{1off}} + \frac{k^*_{2on}}{p + k_{2off}}\right). \end{aligned} \tag{2.25}$$

Normalization

Usually experimental data are normalized such that the fluorescence intensity ranges from 0 to 1. The curve obtained with the analytical solution should show the same behavior to enable comparison between experimental and theoretical data. In the analytical approach the fluorescence intensity is calculated by integrating the concentrations of the free and bound proteins over the bleach spot and dividing this value by the area of the bleach spot. By setting $F_{eq} + C_{eq} = 1$ the intensity for the equilibrated system before the bleach calculates to 1. A prerequisite for the analytic solution it that the bleach spot is small relative to the total cell. The fraction of fluorescence that is lost during bleaching is therefore negligible and the concentrations of free and bound fluorescence will recover to their equilibrated values F_{eq} and C_{eq}. The final height of the recovery curve is hence 1 as demanded.

Combining the above equality with Eq. 2.18 gives the following relationships for the equilibrium concentrations for the one-binding-state model:

$$F_{eq} = \frac{k_{off}}{k^*_{on} + k_{off}} \quad \text{and} \quad C_{eq} = \frac{k^*_{on}}{k^*_{on} + k_{off}}. \tag{2.26}$$

Using the same considerations for the two-binding state model yield the normalization condition: $F_{eq} + C_{1eq} + C_{2eq} = 1$. Combining with Eq. 2.21 gives the following relationships:

$$\begin{aligned}\frac{1}{F_{eq}} &= 1 + \frac{k^*_{1on}}{k_{1off}} + \frac{k^*_{2on}}{k_{2off}} \\ \frac{1}{C_{1eq}} &= 1 + \frac{k_{1off}}{k^*_{1on}}\left(1 + \frac{k^*_{2on}}{k_{2off}}\right) \\ \frac{1}{C_{2eq}} &= 1 + \frac{k_{2off}}{k^*_{2on}}\left(1 + \frac{k^*_{1on}}{k_{1off}}\right). \end{aligned} \tag{2.27}$$

2.3.8 Different scenarios for one-binding state model

The full analytical solution for the FRAP recovery for the one binding state model derived in section 2.3.7 depends on four parameters. These are the free diffusion coefficient (D_f), the size of the bleach spot (w), the pseudo-on rate (k^*_{on}), and the off rate (k_{off}). A more detailed analysis of the parameter space showed that there are simplified models, which describe the solution within a distinct range of the parameters satisfactorily [32].

Timescales for the FRAP recovery
The dynamics of the proteins during a FRAP recovery can be described in terms of two different time scales:

1. The timescale for the diffusion process is defined by the characteristic diffusion time, which can be calculated with Eq. 2.9: $\tau_{1/2} = w^2/D_f$.

2. The average time for a protein to move from one binding site to the next is given by $\tau_d = 1/k_{on}$ (see section 2.3.2).

These two timescales and the ratio of free and bound proteins determine whether the binding state can be described by a simplified model.

Pure-diffusion dominant
For this simplification most of the fluorescent molecules are free and FRAP measures primarily free diffusion of the fluorescent proteins. Under these conditions binding has no influence on the solution and can be ignored. The pure diffusion regime occurs when the ratio of bound to free molecules is $\leq 1\%$:

$$\frac{C_{eq}}{F_{eq}} \leq 0.01 \quad \xrightarrow{Eq.\,2.18} \quad \frac{k^*_{on}}{k_{off}} \leq 0.01 \tag{2.28}$$

Effective diffusion
In this case binding reaction is much faster than the typical time involved in the diffusion process ($\tau_d \ll \tau_{1/2}$). This implies that any location within the bleach spot, the binding rapidly achieves a local equilibrium. Crank (1975) has shown that this case can be described by a simple diffusion equation with a new diffusion coefficient, known as the effective diffusion constant D_{eff}. This constant takes the original diffusion coefficient and the binding rates into account:

$$D_{eff} = \frac{D_f}{1 + (k^*_{on}/k_{off})}. \tag{2.29}$$

The decreased diffusion coefficient $D_{eff} < D_f$ considers the slower movement of the proteins due to the binding events.

Reaction dominant
The last simplified model occurs if diffusion is very fast compared to both, the binding reaction and the timescale of the FRAP experiment ($\tau_d \gg \tau_{1/2}$). After photobleaching the unbound molecules instantly diffuse into the bleach spot and their concentration reaches the equilibrated value. The fluorescence recovery detected by FRAP hence arises not from these free fluorescent proteins but from the bound ones. A bound protein is released after the average binding time ($\tau_b = 1/k_{off}$) and eventually moves out of the bleach spot. The free binding site can now be occupied by a fluorescent protein what will lead to an increase of the fluorescence intensity. To recognize a noticeable influence of the binding sites, the equilibrium concentration of the bound proteins C_{eq} should be significantly large:

$$\frac{F_{eq}}{C_{eq}} = \frac{k_{off}}{k^*_{on}} \lesssim 1. \tag{2.30}$$

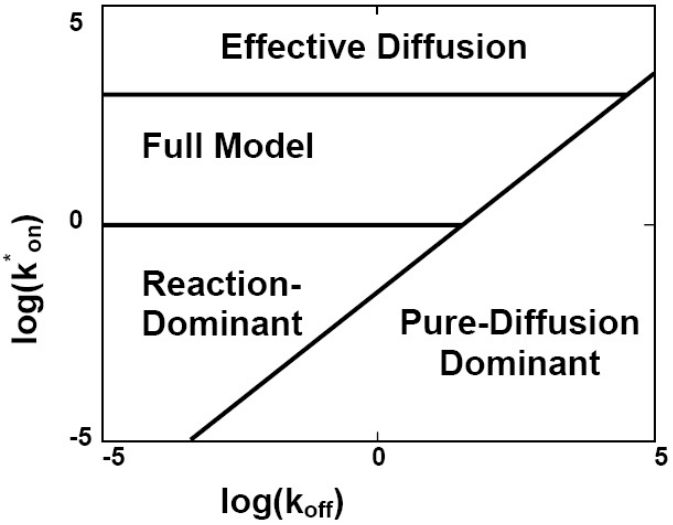

Figure 2.12: ***Localization of the model domains****. The boundaries between the simplified and the full model in the (k^*_{on}, k_{off}) parameter space can be approximated by three lines (from [32]).*

Analysis of the parameter space
The diffusion coefficient and the bleach spot size are parameters that are fairly similar from one FRAP experiment to another. Measured values for the diffusion coefficient range from $\sim 15 - 40\,\mu m^2/s$, and the bleach spot size for most FRAP experiments is on the order of $1\,\mu m$ [32]. On the other hand,

the binding rates for different nuclear proteins can vary strongly. Hence, the behavior of the system is mainly determined by the binding rates. Sprague et al. investigated which simplified model holds for particular combinations of binding rates. For this purpose they assumed a fixed diffusion coefficient $D = 30\,\mu m^2/s$ and a bleach spot radius of $0.5\,\mu m$. The binding rates were varied over a 10^{10}-fold range. For each point in the (k^*_{on}, k_{off}) parameter space they calculated the difference between the solution for the full model and each of the simplified models. They found a simple map in the parameter space to indicate where a simplified model can be used to describe a FRAP experiment (see Figure 2.12).

Typical binding rates of nuclear proteins

The typical values for binding rates of nuclear proteins cover a wide range [32]. Typical off-rates range from $\sim 10^1 s^{-1}$ for nonspecific DNA binding to $\sim 10^{-6} s^{-1}$ for many types of specific binding. Typical on-rates range from $\sim 10^2 - 10^8 M^{-1} s^{-1}$. To calculate the pseudo-on rate the on-rate is multiplied by the equilibrium concentration of bound sites. Considering a specific case, DNA as binding site has a concentration of $\sim 20mM$, so that the pseudo-on rates range from $\sim 2 - 20 \times 10^5 s^{-1}$.

This wide range of the binding rates implicates that for biological system different behavior of the proteins can be expected (see Figure 2.12). In a comprehensive study of FRAP experiments this wide range should be considered by investigating the whole parameter space.

Chapter 3

Methods

The partial differential equations that describe the protein dynamics are numerically solved with the finite element method. In the first section this method and its implementation in MATLAB's PDE toolbox is introduced. The following sections cover an explanation of the developed FramSim and FrapDomain environment for the numeric simulation of FRAP experiments.

3.1 Finite Element Method

3.1.1 Basics

The finite element method (FEM) is one of the most popular ways of solving partial differential equations in various branches of applied science. In essence, the finite element method is a numerical technique which solves the governing equations of a complicated system through a discretization process. In general the FEM can be used to solve two or three dimensional problems. The following explanations concentrate on two dimensions since the protein dynamics in FRAP experiments are restricted to a plane.

Discretization of the geometry - mesh generation

A key requirement of the Finite Element method is the application of a mesh, which subdivides the domain on which the partial differential equations are defined. The process of subdividing a geometric object in a plane into smaller simple elements (triangles) is called triangulation [19]. The accuracy and even the validity of a solution depends strongly on the properties of this mesh.

At first step a geometry in $\mathbb{R}^2$ is given via a discretization of its boundary. The boundary is described as a list of segments, with given start-point and end-point coordinates. Then an incremental method is used to generate

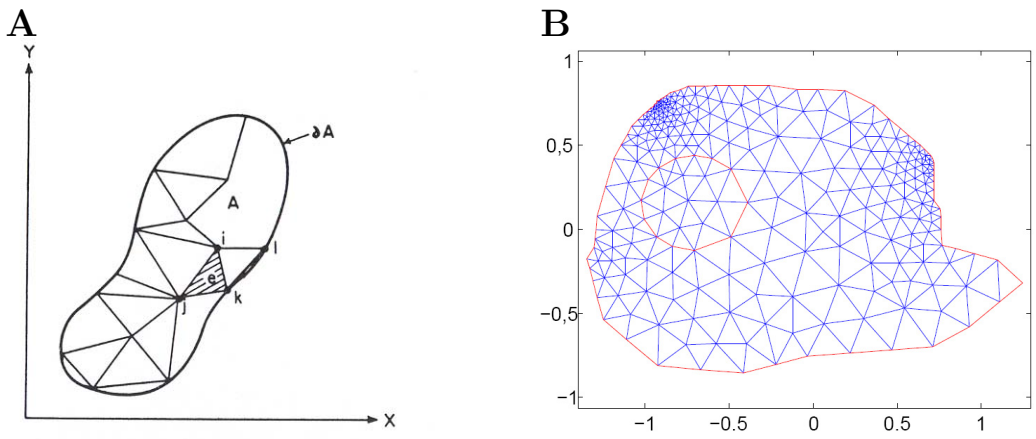

Figure 3.1: ***Finite element geometry A*** *The domain A is discretized in terms of finite elements. The triangular element e has nodes i, j, k (from [2]).* ***B*** *Triangular mesh generated by Matlab.*

the interior mesh which is described by a set of vertices. As the result the domain of interest (A) is separated by imaginary lines into a number of finite elements (triangles) as in Figure 3.1. Those elements are assumed to be interconnected at a discrete number of nodal points, the vertices of the triangles. An advantage of FEM is that it can be applied even if the region of interest is complex because even complex geometries can be partitioned into simple elements.

Matlab uses an implementation of the Delaunay triangulation algorithm to calculate a triangular mesh on the defined geometry. The triangles of the mesh that are generated with this triangulation method satisfy the so-called empty circle criterion. This criterion means that a circle drawn through the vertices of a triangle, the so called circum circle, will contain no other vertices. The Delaunay triangulation maximizes the minimum angle of all triangles in the mesh. The triangles formed by this method are as equilateral as possible. The equilateral shape is very important since it reduces potential numerical precision problems and visualization artifact, which might be created by long slim triangles.

Mesh refinement

The number of triangles within a mesh can influence the accuracy of the numeric solution immensely. A mesh with more and smaller elements will increase the accuracy of the results but also increases the calculation time. There are several approaches to refine an existing mesh, i.e., increase the number of finite elements. Two simple methods are implemented in *FrapSim*. First, the whole mesh can be refined uniformly by dividing each triangle into

four smaller ones. This is done by connecting the midpoints of each side of the initial triangle. Second, the mesh can be refined only in selected regions. This is particularly important if the solution has geometric features like localized strong gradients. Then it is more economical to refine the mesh selectively, i.e., only where it is needed. A selective refined mesh is a convenient way to increase the accuracy of the solution without wasting computational resources.

Triangle quality

There is no generally agreed definition of how to measure the triangle quality. A widely used criterion measures the likeness of the triangle to the reference shape, i.e., the ideal shape a finite element should have. This is done by comparing the triangle area A to the area of an equilateral one[1]. For a given triangle T of area A and side length h_1, h_2, and h_3 the quality can be measured by

$$q(T) = \frac{4\sqrt{3}A}{h_1^2 + h_2^2 + h_3^2}. \tag{3.1}$$

The function $q(T)$ is one for equilateral triangles (all inner angles are $\frac{\pi}{3}$) and zero for flat triangles (at least one inner angle is zero). q decreases as the element became worse and as long as $q > 0.6$ the triangle is considered to be of acceptable quality [33].

Discretization of the PDE - Variational problem

The second step in the solution process is the discretization of the PDE on the mesh and the building of an equation for the discrete approximation of the solution. The unknown exact solution u is discretized by saying it should be piecewise linear on each triangle, hence the solution u can be described by a linear approximation u_h

$$u_h(x) = \sum_{i=1}^{N} U_i \phi_i(x), \tag{3.2}$$

where ϕ_i are some special piecewise linear basic functions, U_i scalar coefficients, and N the number of nodal points. There are many choices for the test functions [19]. The implementation of the FEM in Matlab uses basic function a ϕ_j, which takes the value 1 at the node point j and the value 0 elsewhere. In two dimensions these functions form a pyramid-like shape on each of the vertices (Figure 3.2). The solution vector U contains the coefficients of u_h, which are the values of u_h at each node x_i since $u_h(x_i) = U_i$. The elements of U are the basic unknown parameters which have to be calculated.

[1] Area of an equilateral triangle with side length b: $(\sqrt{3}/4)b^2$

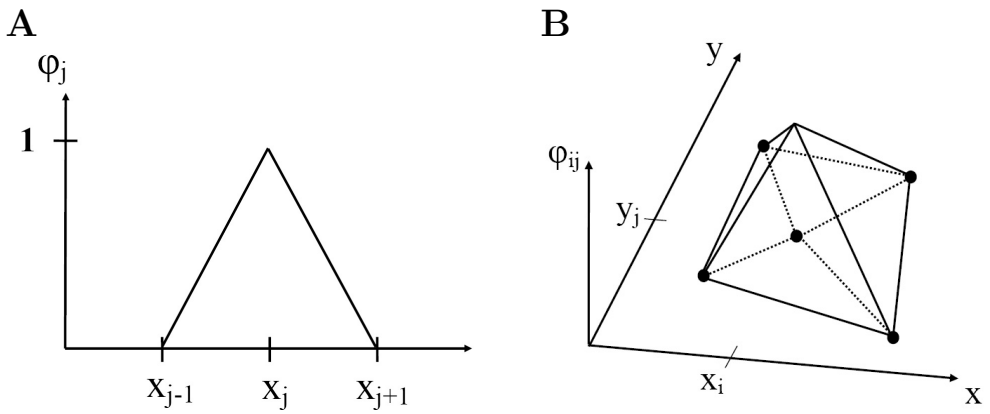

Figure 3.2: ***The basic function for the FEM.*** ***A*** *The basic function ϕ_j is one at the nodal point j.* ***B*** *The function ϕ_{ij} is pyramid-like in 2D.*

The equation of u_h is tested against all possible functions v of the class of the continuous piecewise polynomials in order to estimate the best approximation of u . The functions v are usually called *test functions*. This is done in the FEM by a reformulation of the given differential equation as an equivalent variational problem. This variational form is then projected onto the mesh and the solution of the resulting system of equations yields the wanted parameters.

3.1.2 Matlab's PDE Toolbox

The Partial Differential Equation (PDE) Toolbox extends the MATLAB technical computing environment with powerful and flexible tools for the study and solution of PDEs in two-space dimensions and time. It provides a set of command line functions and a graphical user interface (GUI) for solving PDEs using the Finite Element Method (FEM). The single steps during the modeling and solution process can be done either with the GUI or by using command line functions. Even a combination is possible, parts of the modeling can be done in the `pdetool` GUI and then made available in the Matlab workspace through the export facilities of the GUI [33]. The flexibility of this design enables the user to develop own tools implementing the required commands from the PDE toolbox. In addition Matlab provides with *GUIDE* (Graphical User Interface Development Environment) a convenient tool for the development of own graphical user interfaces. Those were the deciding points to choose Matlab for the development of *FrapSim*.

3.2 *FrapSim*

FrapSim provides a graphical user interface for the modeling and simulation of a FRAP experiments. The most important features are

Definition of the geometry and the mesh
The basic elements that set up a FRAP experiment can be defined individually and can have arbitrary geometries. The *nucleus* defines the outer boundary of the geometry. The *nucleolus* is accessible by diffusion but there are no binding sites within it. The *binding sites* can either be set to be distributed in the whole nucleus or be defined with a separate geometry. The photobleaching is performed within the *bleach spot* and the recovery of fluorescence is measured in the *recovery spot*. After the definition of the geometry the user can initialize the mesh. In order to increase the accuracy of the solution refinements of the whole mesh are possible just as refinement of selected regions.

Photobleaching methods
FrapSim can simulate FRAP, iFRAP (inverse FRAP), and FLIP (Fluorescence Loss In Photobleaching) experiments with either an uniform or a Gaussian bleaching profile.

Solution
The user can define the time interval for the numerical solution. The final step is the solving of the PDE problem which results in the time dependent concentrations of the free and bound proteins. The time-course of the concentrations during the FRAP recovery can be animated with a separate GUI. The simulated recovery curve can be stored or exported to the Matlab workspace for further calculations. In addition the analytic solution based on the defined parameters can be calculated.

3.2.1 Architecture

The *FrapSim* environment consists of a set of classes (see Appendix A.2) which can be divided into two groups:

- **Visual classes** which involve a graphical user interface for interaction with the user. These classes all begin with GUI (except FrapSim) and consist of two files: the GUI M-file that controls the GUI and determines how it responds to a user's action, and the GUI FIG-file, which contains a complete description of the GUI layout.
- **Auxiliary classes** which the user can not use directly.

Matlab provides a mechanism, called the *handles structure*, to manage the data of a GUI. Matlab stores all relevant data that describes the components of a GUI in this structure. In addition this structure is useful to save every shared data. A FRAP experiment in *FrapSim* is described by a large number of variables. Using each of these variables as a separate input parameter for a class would result in a long and confusing list of input parameter. Thus, most of the auxiliary classes have the *handles structure* of the overall GUI as an input parameter. At the beginning of each class the used variables are assigned to temporary variables to indicate which variables are currently used.

The process of defining and solving the PDE problem is done in several steps. A number of data structures define different aspects of the problem, and the various processing stages produces new data structures. In Figure A.3 a typical workflow is represented graphically.

3.2.2 Geometry

The first important steps in the modeling process is the definition of the geometry that describes the problem.

Constructive solid model

The Matlab PDE Toolbox uses the Constructive Solid Geometry (CSG) model paradigm to describe the geometry. The geometric model consists of overlapping solid objects. Each object is identified by an unique name stored in one character column in the *Name Space Matrix* `ns`. The *Geometry Description matrix* `gd` describes the graphical properties of the model. Each column in `gd` corresponds to one solid object, the first row determines the object type. The other rows specify the geometry itself. Four different types of solids can be defined: *circular objects* specified by 1, *polygonal objects* specified by 2, *rectangular objects* specified by 3, and *elliptic object* specified by 4. Each solid defines a set of points. The names of the solid objects can then be used in the *set formula* `sf` to refer to their points and define relationships between them by set operators:

- $+$; the set union operator.
- $-$; the set difference operator.
- $*$; the set intersection operator.

The resulting geometric model Ω is the set of points for which the set formula evaluates to true. The partial differential equation is solved over this domain.

The nuclear boundary defines the outer boundary of the system. To ease the definition of the geometry it is possible to define the other elements larger than the nucleus, e.g., for a bleach strip over the whole nucleus. *FrapSim* considers for the further calculations only the part of this element that is within the nucleus. This is achieved by an intersection of the defined geometry with the nucleus. For example, a geometry consisting of the nucleus (N) and the bleach spot (BS) is described in the `sf` by $(N\,S + BS) * N\,S$.

In *FrapSim* the user can directly define rectangular or elliptic objects, the matrices describing the CSG Model are automatically created. In addition it is possible to define arbitrary geometries in the PDE toolbox and import the CSG model into *FrapSim*.

Decomposed geometry

The CSG Model is the way the geometry of the problem is defined by the user. For further steps another geometry description has to be created. The **Decomposed Geometry** is created from a CSG model with the the function `decsg`. In this model the geometry is described as a set of disjoint minimal regions (also referred to as subdomains) bounded by edge segments. Each edge segment of the minimal regions is stored in a column in the *decomposed geometry matrix* `dl`. The edge segments between two minimal regions are called border segments, the ones defining the outer boundary as boundary segments. Rows six and seven of *dl* contain the labels of the minimal regions the particular edge segment separates. Since the region outside the defined geometry is labeled with a zero, boundary segments have a zero in one of these rows.

The *boolean table* `bt` relates the original solid objects to the minimal regions. A column in `bt` corresponds to the column with the same index in `gd`. A row in `bt` corresponds to a minimal region index.

3.2.3 Boundary conditions

The boundary conditions are specified by a *boundary condition matrix* `b` which is given as a function on the boundary segments. The toolbox can treat either generalized Neumann boundary conditions (Robin boundary conditions) or Dirichlet boundary conditions.

For each column in the *decomposed geometry matrix* there must be a column in the *boundary condition matrix* `b`. The columns in `b` which correspond to a boundary segment have a special format to describe the boundary conditions on this segments. Whereas the columns in `b` that corresponding to a border segments can contain arbitrary values. For the implementation in

FrapSim zeros are assigned. The mathematical model that describes a FRAP experiment has Neumann (no-flux) boundary conditions (see section 2.3.5). This conditions have to be defined only for the boundary segments. *FrapSim* checks the decomposed geometry matrix `dl` column by column deciding whether this segment corresponds to a boundary segment or not and adds the corresponding column to `b`.

3.2.4 Mesh

The PDE toolbox has mesh generating and mesh refining facilities that are used by *FrapSim*. Matlab uses a Delaunay triangulation algorithm to calculate a triangular mesh on the defined geometry. A mesh is defined by three matrices of fixed format that contain information about the mesh points (*point matrix* `p`), the boundary segments (*edge matrix* `e`), and the triangles (*triangle matrix* `t`).

The *FrapSim* environment has a function for global uniform mesh refinement. In addition, it enables the selective refinement of some geometric elements.

- **Bleach spot** or **Recovery spot**.
- **Bleach spot boundary**. In this part of the geometry the concentration gradient is very strong after the photobleaching.
- **Refinement spot**. The user can define an arbitrary region for selective mesh refinements. It can be used to asses the influence of selective refined meshes on the numeric solution.

The quality of one triangle of the mesh can be assessed with the Matlab function `pdetriq`, which calculates the quality according to Eq. 3.1. *FrapSim* uses this function to calculate the mean value for the whole mesh. The mesh quality can normally be improved with the function textttjigglemesh by adjusting the node point positions.

3.2.5 Initial conditions

After the definition of the geometry and the mesh the initial conditions of the PDE problem can be set up. They are described by a column vector u_0, which assigns a value to each point of the mesh.

Equilibrated system
One of the assumptions during the derivation of the mathematical model

was that the biological system has reached equilibrium before photobleaching. Hence, *FrapSim* calculates the equilibrated concentration for each of the variables based on Eq. 2.18 and Eq. 2.21 before any technique is applied.

In the equilibrated system the free diffusing proteins are homogeneously distributed in the nucleus. At locations with a binding site an exchange with this immobile complex occurs, i.e., a specific amount of proteins is bound. *FrapSim* calculates the equilibrium concentrations according to this behavior:

- Without a binding site the concentration of the free proteins is set to 1 for each mesh point.
- With one binding site, the value for the free proteins is set to 1 in the whole nucleus. The concentration for the binding site is calculated according to Eq. 2.18. This value is assigned to each point that is within the binding site, outside it is set to zero.
- With two binding sites Eq. 2.21 is used to calculate the equilibrated concentrations. The concentrations for bound proteins are set to zero outside their defined geometry.

Uniform bleaching profile
The bleaching process alters the calculated equilibrated system. If techniques with a uniform bleaching profile are chosen, all concentration within the bleach spot are set to a value

$$value_{new} = bleachRate * value_{old},$$

where *bleachRate* defines the amount of unbleached molecules, e.g., for a full bleach during a FRAP experiment *bleachRate* is set to 0. The photobleaching is performed only on the subdomains which build up the bleach spot. The corresponding values can be found out by looking at the *boolean table* `bt` (see section 3.2.2).

Gaussian bleaching profile
A Gaussian distribution in two dimensions is determined by the following equation:

$$f_{gauss}(x,y) = e^{-\frac{(x-\mu_x)^2}{2\sigma_x^2}} \cdot e^{-\frac{(y-\mu_y)^2}{2\sigma_y^2}}, \tag{3.3}$$

where μ_x and μ_y determine the maximum value in x and y direction, and σ_x^2 and σ_y^2 are the corresponding variances

In *FrapSim* bleaching with a Gaussian profile is only possible for elliptic bleach spots. The values of the bleach spot geometry are the basis for the

estimation of the parameters off the Gaussian distribution. The coordinates of the center of the ellipse are used as the mean values, the values of the x and y semi-axes are used as values for the variance. The concentration after the bleach is calculated by multiplying each value of the equilibrated system with $(1 - f_{gauss})$ times the bleach rate:

$$value_{new} = value_{old} * (1 - f_{gauss}) * bleachRate.$$

Here the *bleachRate* distinguished the amount of photobleached molecules. A full bleach is here performed with a value of 1.

3.2.6 PDE coefficients

FrapSim uses the Matlab function `parabolic` to solve the reaction-diffusion equations that describe a photobleaching experiment. `parabolic` calculates the solution for the FEM formulation of the system PDE problem on the user defined geometry Ω in two dimensions:

$$\underline{d}\frac{\partial u}{\partial t} - \nabla \cdot (\underline{c} \otimes \nabla u) + \underline{a}\, u = f \text{ on } \Omega. \tag{3.4}$$

Matlab allows for specifying the PDE coefficients for each subdomain separately. So it is, e.g., possible to define binding rates only for a specific part of the geometry. The coefficients d, c, a, and f can be represented in different ways. For the implementation in *FrapSim* they are stored as a sequence of Matlab text expressions separated by exclamation marks (*Coefficient Matrices*). Each of these text expressions estimates the value of the coefficient for the subdomain with the corresponding label. The number of expressions must be equal to the number of subdomains. For a detailed description of the calculation of the PDE coefficients in *FrapSim* see Appendix A.4.

3.2.7 Recovery curve

In *FrapSim* the fluorescence intensity is measured with a simple numerical integration of the protein concentration over the recovery spot. This corresponds to a measurement with a stationary laser beam with an uniform intensity profile in a real experiment. For the numeric integration the area of each finite element is multiplied with its function value, i.e., the concentration of the free and bound proteins. These values are summed up for the whole recovery spot yielding the fluorescence intensity for one point in time. The whole recovery curve is obtained by repeating the integration for the whole time interval. Finally, the calculated recovery curve is normalized with respect to the initial fluorescence before photobleaching.

Loss of fluorescence during the bleaching
The simulated data is normalized with respect to the *initial* fluorescence intensity before photobleaching. Hence, the loss of fluorescence intensity during the bleaching is the difference between the pre-bleach value of the recovery curve and its final value. This value can be calculated with a simple approach if homogeneously distributed fluorescent proteins can be assumed. The measured fluorescence intensity is proportional to the concentration of fluorescent molecules within the bleach spot and can be normalized to be 1 before the photobleaching. The photobleaching process reduces the total number of fluorescent molecules by making those within the bleach spot invisible. The reduced number of fluorescent proteins yields a smaller final value of the fluorescence intensity F_∞. The actual final height is proportional to the ratio of the number of of unbleached molecules after the bleaching to the total number of proteins. Thus F_∞ can be calculated with the ratio of the area that is not bleached to the total area of the nucleus:

$$F_\infty = \frac{A_{NS} - A_{BS}}{A_{NS}}, \tag{3.5}$$

where A_{NS} is the area of the nucleus and A_{BS} is the area of the bleach spot.

3.2.8 Analytic solution

The analytic solution can be calculated in *FrapSim* with Eq. 2.24 or Eq. 2.25 if a circular bleach spot is defined. The user defined parameters from the current simulation are used to estimate the necessary parameters for the calculation: the diffusion coefficient D_f, the bleach spot radius w, the binding rates, and the time list vector. The inverse Laplace transformation is done numerically with the Matlab routine `invlap` [18].

3.3 *FrapDomain*

FrapDomain is a graphical tool which enables the comparison of FRAP recovery curves over the whole range of the (k^*_{on}, k_{off}) parameter space. It can either be called directly from the *FrapSim* environment or from the Matlab command line. The parameters describing the numerical model are passed to *FrapDomain* for the first case or can be imported from the Matlab workspace for the latter. *FrapDomain* assumes an one binding-state model for the analytic and numeric solution, the corresponding binding rates can be varied over a user defined range. A number of numeric solutions and analytic solutions

can be calculated for the whole parameter space. Two solutions can then be compared by calculation the sum of residuals between the two curves.

3.3.1 FRAP recovery times

For a comprehensive analysis the FRAP recovery curves should be compared over the full range of the recovery process. The fluorescence intensity is assumed to be fully recovered if it has reached 99% of its final value. The corresponding time the system needs is denoted as *FRAP recovery time*. The estimation of the recovery time for each (k^*_{on}, k_{off}) is done with the analytical solution $frap(t)$, which is the fluorescence intensity at time t. Matlab provides a function `fzero(f,[`t_0 t_1`])` that tries to find a zero of `f` in the interval $[t_0\ t_1]$. The value returned by `fzero` is near a point where `f` changes sign. By setting $f = frap(t) - 0.99$ the returned value is the point in time when the recovery gets greater than 99%. The search interval is set to $[10^{-5}\,1/s,\ 10^{15}\,1/s]$, which is more than sufficient to cover very fast and very slow recovery processes and restricts the search to times $t \geq 0$. The FRAP recovery times are stored in a matrix `t99`, which is then used to determine the time interval for the calculation of the recovery curves.

3.3.2 Sum of residuals - goodness of agreement

The goodness of agreement between two solutions is quantified by the sum of residuals of the two recovery curves. This value is defined as the sum of the absolute values of the difference between the two recovery curves $frap_1$ and $frap_2$ at every point in time:

$$R = \sum_{t=1}^{m} \Big| frap_1(t) - frap_2(t) \Big|, \tag{3.6}$$

where m number of elements in the time list vector.

3.4 *FrapFit*

The analytic solution derived in section 2.3.7 can be used for the fitting of experimental data and the estimation of the underlying parameters. *FrapFit* is a tool developed in Matlab which uses the Matlab function `lsqcurvefit` to solve the data-fitting problem in the least-squares sense. With given input data *tdata* (time points) and observed output data *ydata* (fluorescence intensity) it finds the best coefficients C to minimize the function

$$\frac{1}{2}\sum_{i=1}^{m}\left(frap(C, tdata_i) - ydata_i\right)^2, \tag{3.7}$$

where $tdata$ and $ydata$ are vectors of length m and $frap(C, xdata)$ is the vector-valued function of the analytic solution. Sprague et al. have developed a method to conduct FRAP experiments on GFP tagged proteins which are assumed to undergo binding events [32]. First of all, a FRAP experiment for GFP alone is performed. It is assumed that the GFP diffuses freely through the nucleus without undergoing any binding events. Hence, the dynamics of this protein are only determined by its diffusion coefficient. The fluorescence recovery for free diffusion has been extensively analyzed. For a circular bleach spot with a radius w and an infinite nucleus a closed solution exists:

$$\begin{aligned} frap(t) &= \left(I_0\left(\frac{\tau_d}{2t}\right) + I_1\left(\frac{\tau_d}{2t}\right)\right) e^{-\tau_d/2t}, \\ \text{where } \tau_d &= \frac{w^2}{D_f}, \end{aligned} \tag{3.8}$$

where D_f is the diffusion coefficient, τ_d is the characteristic diffusion time, I_0 and I_1 are modified Bessel functions. After the estimation of the diffusion coefficient of GFP alone the diffusion of the tagged protein can be calculated by considering the increased molecular weight (see section 2.3.1). Now the actual experiment can be performed. The diffusion coefficient of the tagged protein can be assumed to be a priori knowledge which reduces the number of unknown parameters and eases the data fitting.

The structure of the *FrapFit* environment follows this approach. The user can import experimental data together with the corresponding time list vector into the environment. It is possible to fit the data either to the diffusion model or to the one-binding state model with a known diffusion coefficient. For the latter the user can specify a starting guess for the binding rates.

Chapter 4

Results and discussion

In the first section the accuracy of the numerical solution is tested. The sensitivity of the FEM with respect to both the mesh size and the underlying parameters is assessed. An efficient mesh refinement strategy in order to obtain reliable numeric results is presented. In the following section the numerical model is used to simulate different experimental setups in order to quantify their impact on the FRAP recovery curve. It is of particular importance to consider this influence during the evaluation of experimental data, otherwise a misinterpretation of the data will be the result.

4.1 Program validation

The first important step before any simulation can be done is the validation of the numeric model, i.e., to assess the accuracy and reliability of the numeric solution. I used a one-binding-state model for the validation of the numeric solution. A second binding site had only complicated the interpretation of the results and brought no new insight. The recovery times and sum of residuals were calculated for the whole parameter space of the binding rates k^*_{on} and k_{off}, which were both out of the interval $[10^{-5}\,s^{-1}, 10^{5}\,s^{-1}]$. In order to resolve this huge range I used logarithmic scaled axis with 20 equidistant points, which resulted in a parameter space with a total of 400 points. The recovery curves were calculated for 100 equidistant time points over the full range of recovery to 99%. To test the accuracy of the numerical solution I used *FrapDomain* to compare the results for a simple numeric model with the analytical solution. For the numerical model I assumed a circular nucleus with a radius of $R_{NS} = 7.5\,\mu m$, which is a realistic value for living cells (see Figure 2.1). The bindings site is homogeneously distributed in the whole nucleus. I set the diffusion coefficient equal to a realistic value for GFP in

nucleoplasm of $D_f = 30\,\mu m^2/s$. The bleaching is performed with a uniform intensity profile in a concentric bleach spot with a radius of $w = 0.5\,\mu m$. I used these values for all numerical simulations, if different values were used it is denoted explicitly.

The numeric model meets the most important assumptions which are essential for the solution of the analytic model. Thus, the analytic solution can be used to quantify the numeric results. In addition, the parameters of the numerical model, e.g., the nucleus size, the bleach spot radius and the diffusion coefficient, were realistic values for a FRAP experiment and the simulated results could be compared to real experimental data.

4.1.1 FRAP recovery times

To test the implementation of the calculation of the FRAP recovery times I calculated them for the whole parameter space and plotted their distribution as a function of the off- and pseudo-on rates. The accuracy of the computation was tested by calculating the value of the analytic solution for the estimated recovery times. The statistical analysis of this data yielded a mean value of 0.99 with a standard deviation of 1×10^{-15}.

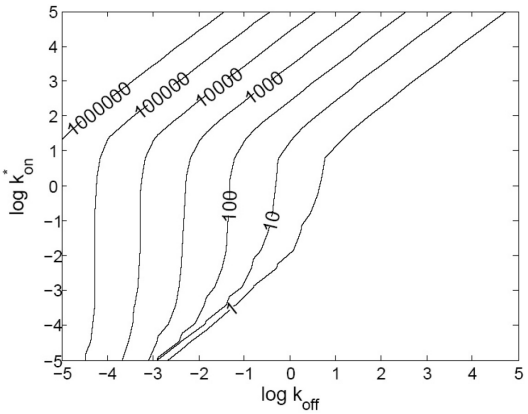

Figure 4.1: ***FRAP recovery times****. The contour plot shows the recovery times for the analytic solution as a function of the binding rates.*

The distribution shows the same behavior as the one calculated by Sprague et al. [32]. The statistical analysis shows that the demanded recovery of the fluorescence intensity to 99% of its final value is satisfactorily fulfilled.

4.1.2 Comparison of analytic and numeric solutions

The first simulation was done to get an estimate for the accuracy of the numeric solution calculated with the FEM approach. For this purpose, I used *FrapDomain* to compare the results of the numeric model discretized by the initial mesh with the results of the analytic solution.

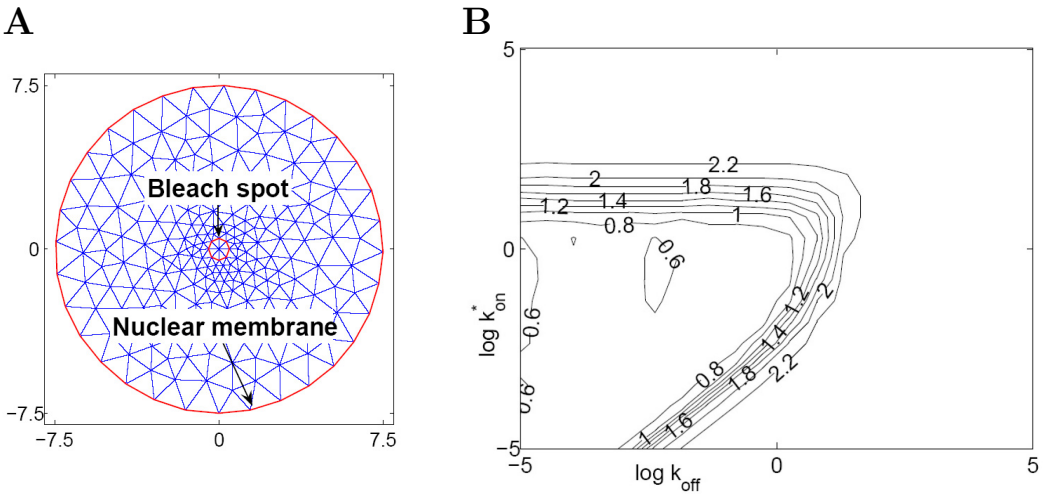

Figure 4.2: ***Numeric solution with initial mesh.*** ***A*** *Geometry of the model with nucleus (large red circle), bleach spot (small circle), and the mesh.* ***B*** *Sum of the residuals calculated with respect to the analytical solution.*

Figure 4.2B shows the distribution of the sum of the residuals as a function of the binding rates. Generally, it can be said that the accuracy of the numerical solution shows a strong dependency on the binding rates and can be summarized in terms of the simplified models shown in Figure 2.12.

Table 4.1: Summary of the numeric solution with the initial mesh. Δ_{Total} *and* Δ_{BS} *are the numbers of finite elements of the whole mesh and the bleach spot,* $\text{Resid}_{\text{min}}$ *and* $\text{Resid}_{\text{max}}$ *the minimum and maximum values of the sum of the residuals.*

Scenario	Δ_{Total}	Δ_{BS}	$\text{Resid}_{\text{min}}$	$\text{Resid}_{\text{max}}$
Initial mesh	418	8	0.56	2.38

The results were only acceptable for the reaction dominant regime and therefore further investigations are necessary in order to improve the quality of the

solution. I concentrate on two major factors which both have a large impact on the solution. Those factors are the number of finite elements of the mesh and the size of the nucleus. An increased mesh size leads to a larger number of nodal points describing geometry of the PDE problem. This reduces the error due to the discretization. By increasing the nucleus size the numeric solution comes more closer to the analytic approach by reducing the influence of the nucleus membrane.

4.1.3 Influence of the mesh size

To investigate the influence of the mesh size on the recovery curve more in detail I calculated the numeric solution for the same model discretized with meshes of different size.

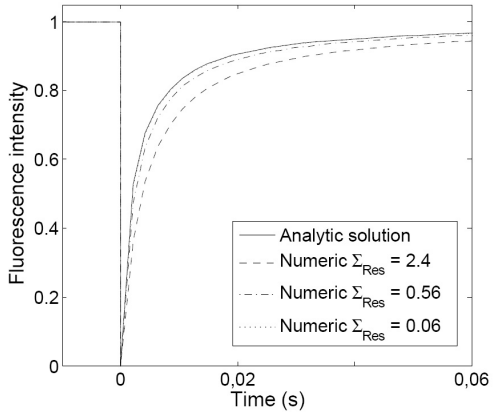

Figure 4.3: ***FRAP recovery curves for different mesh sizes****. The sum of residuals for the numerical solutions were calculated with respect to the analytic solution (solid line).*

In order to save computation time the recovery curves were not calculated for the whole parameter space but only for one pair of binding rates. The worst agreement between the numeric and analytic solution is within the pure-diffusion regime (Figure 4.2). So the decision was made to values that describe this behavior ($k^*_{on} = 10^{-3}s^{-1}$, $k_{off} = 10^3 s^{-1}$). The corresponding recovery time for these binding rates was calculated with *FrapDomain* ($t_{99} = 0.21$). I did the first calculation with the mesh obtained directly after the initialization. For the following simulations I refined successively either the whole mesh or just the mesh of the bleach spot. After the mesh refinement I used the `jiggle` function to further improve the mesh quality (see section 3.2.4) and calculated the recovery curve for each mesh.

Table 4.2: Influence of mesh refinements on the quality of the solution. Total *and* BS *are the numbers of refinement cycles for the whole mesh and the bleach spot,* Δ_{Total} *and* Δ_{BS} *the numbers of finite elements for the whole geometry and the bleach spot,* Quality *the mean value of the triangle quality,* Residuals *the sum of the residuals,* Change *the difference of the sum of residuals in % compared to the previous value.*

Mesh Refinement					**Residuals**	
Total	BS	Δ_{Total}	Δ_{BS}	Quality	Residuals	Change
0	0	418	8	0.965	2.386	
0	1	470	32	0.952	1.615	-32%
0	2	666	128	0.940	0.644	-60%
0	3	1260	512	0.941	0.297	-53%
0	4	3136	2048	0.952	0.141	-52%
0	5	9952	8192	0.965	0.058	-58%
1	0	1672	32	0.985	1.211	
1	1	1814	128	0.979	0.825	-31%
1	2	2352	512	0.972	0.360	-56%
1	3	4244	2048	0.967	0.169	-53%
2	0	6688	128	0.993	0.590	
2	1	7160	512	0.989	0.396	-32%
2	2	8986	2048	0.984	0.189	-52%
3	0	26752	512	0.995	0.243	
3	1	28440	2048	0.993	0.168	-31%

Two simple rules can be used to describe correlation between the mesh refining strategy and the sum of the residuals:

- The first refining of the bleach spot reduces the residuals to $\sim 70\%$ of their old values. Each further refining of the bleach spot reduces the residuals again by $\sim 55\%$.
- Each refinement of the whole mesh reduces the residuals by $\sim 50\%$

With these rules the surprising result shown in Figure 4.4 can be explained. In this figure the sum of the residuals is plotted as a function of the number of finite elements within the bleach spot. This is done for the initial mesh with a

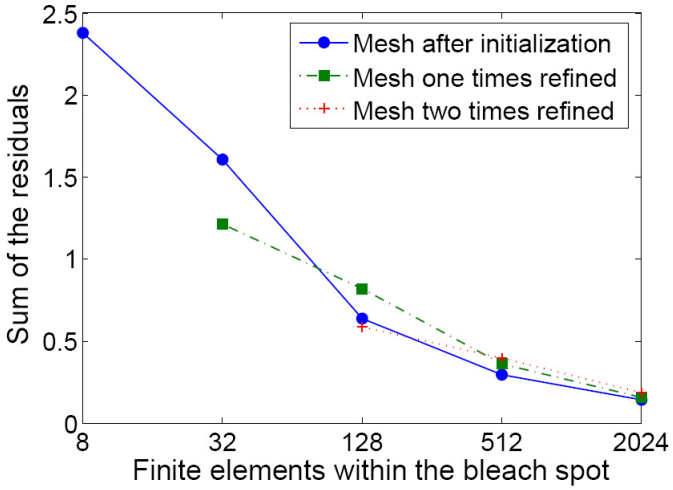

Figure 4.4: ***Dependence of the residuals on the mesh size****. The sum of residuals is calculated for different mesh sizes and plotted as a function of the number of finite elements within the bleach spot.*

successively refined bleach spot as well as for meshes which were first totally refined and then selectively refined at the bleach spot. The numeric solution for a distinct number of elements within the bleach spot is most accurate for the initial mesh with a refined bleach spot, except if the mesh was achieved by refinements of the whole mesh. For example, the initial mesh has 8 elements within the bleach spot. A mesh with 128 elements within the bleach spot can then be generated either with 2 selective refinements of the bleach spot or with one total and one selective refinement. The first approach results in a reduction of the residuals to $R = 0.7 \times 0.45\, R_0 = 0.315\, R_0$, whereas the second reduces the residuals only to $R = 0.5 \times 0.7\, R_0 = 0.35\, R_0$. This is surprising since the initial mesh with a selective refined bleach spot has the smallest total number of finite elements. The computation time is proportional to the number of finite elements. Hence, the successive refinement of the bleach spot yields solutions with the best accuracy and the fastest computation.

Mesh refinement in circular regions

The selective refinement of the mesh of the bleach spot yields promising results. The next question that arose was if a selective refinement of the bleach spot and the neighboring finite elements leads to a further improvement of the accuracy. *FrapSim* provides the possibility to define an additional geometric element, named mesh refine spot, which can be used for selective mesh refinements. I used the same model as for the previous calculations and de-

fined in addition a concentric circular mesh refine spot with radius R_{MR}. I varied R_{MR} from $1.0-3.0\,\mu m$ and refined only the mesh of the refine spot. The refinement was done until either the total number of finite elements was around 10,000 or the number of finite elements within the bleach spot was 512.

Table 4.3: Summary of the calculations with different mesh refine spots. R_{MR} *is the radius of the mesh refine spot,* Δ_{Total} *the total number of finite elements,* Δ_{BS} *the number of finite elements of the bleach spot,* Quality *the mean triangle quality,* Residuals *the sum of the residuals.*

R_{MR} (μm)	Δ_{Total}	Δ_{BS}	Quality	Residuals
-	3136	2048	0.952	0.141
1.0	7264	1792	0.949	0.231
1.5	6998	512	0.963	0.185
2.0	7342	512	0.976	0.176
3.0	12486	512	0.973	0.169

With increasing size of the refinement spot the results get slightly better but the number of triangles increases disproportionally and results in a much longer computation time. This result confirms the previous observations that the best results were obtained by refining only the bleach spot.

Mesh refinement of the bleach spot boundary

The photobleaching process introduces a steep concentration gradient of the fluorescent proteins at the boundary of the bleach spot. A finer mesh in this part of the geometry might, thus, be important for an accurate simulation of the protein dynamics. I calculated the recovery curves for meshes with successively refined finite elements at the boundary of the bleach spot. Again, the sum of the residuals was calculated by comparing the numerical results to the analytic solution. The results are summarized in Table 4.4. They are very promising since a value for the sum of residuals smaller than 0.1 belongs to recovery curves that can be considered to be equal.

Table 4.4: Influence of mesh refinements of the bleach spot boundary. N_{bound} *is the number of points on the bleach spot boundary,* Residuals *the sum of the residuals,* Change *the difference in % compared to the previous value.*

Δ_{Total}	Δ_{BS}	N_{bound}	Quality	Residuals	Change
418	8	8	0.965	2.386	
470	24	10	0.946	1.325	-44.5%
534	49	17	0.935	0.760	-42.7%
688	97	28	0.922	0.546	-28.1%
922	175	41	0.908	0.370	-32.3%
1214	298	63	0.899	0.229	-38.0%
1594	473	95	0.893	0.125	-45.5%
2354	808	151	0.885	0.068	-45.5%
3252	1229	218	0.880	0.025	-62.6%
4694	1884	341	0.876	0.011	-55.2%
6910	2911	495	0.872	0.011	-3.5%

4.1.4 Influence of the nucleus size

To assess the influence of the nucleus size I assumed a circular bleach spot of fixed size ($w = 0.5\,\mu m$). I used two circular nuclei with different radii for the simulations. The first nucleus had a radius of $R_{NS} = 7.5\,\mu m$ and the second a radius of $R_{NS} = 50\,\mu m$.

Table 4.5: Influence of nucleus size on the numerical solution.
N_{bound} *is the number of points on the bleach spot boundary,* T_{calc} *the computation time (see appendix A.1 for computer specification).*

Scenario	Δ_{Total}	Δ_{BS}	N_{bound}	T_{calc}	$Resid_{min}$	$Resid_{max}$
Small nucleus & refined BS	3142	2048	128	6.0 h	0.09	0.46
Large nucleus & refined BS	3516	2048	128	6.7 h	0.0024	0.19
Large nucleus & refined boundary	3208	1112	186	6.5 h	0.0017	0.07

The area of the latter is $R_{NS}{}^2/w^2 = 10^4$ times larger than the one of the bleach spot. Thus, the important assumption of the analytic solution that the nucleus has to be large compared to the bleach spot can be considered to be met for this case. I started with a simulation with the small nucleus and refined the mesh of the bleach spot four times. Then the same procedure was done with the large nucleus. For the last simulation I used the large nucleus and refined just the mesh at the bleach spot boundary.

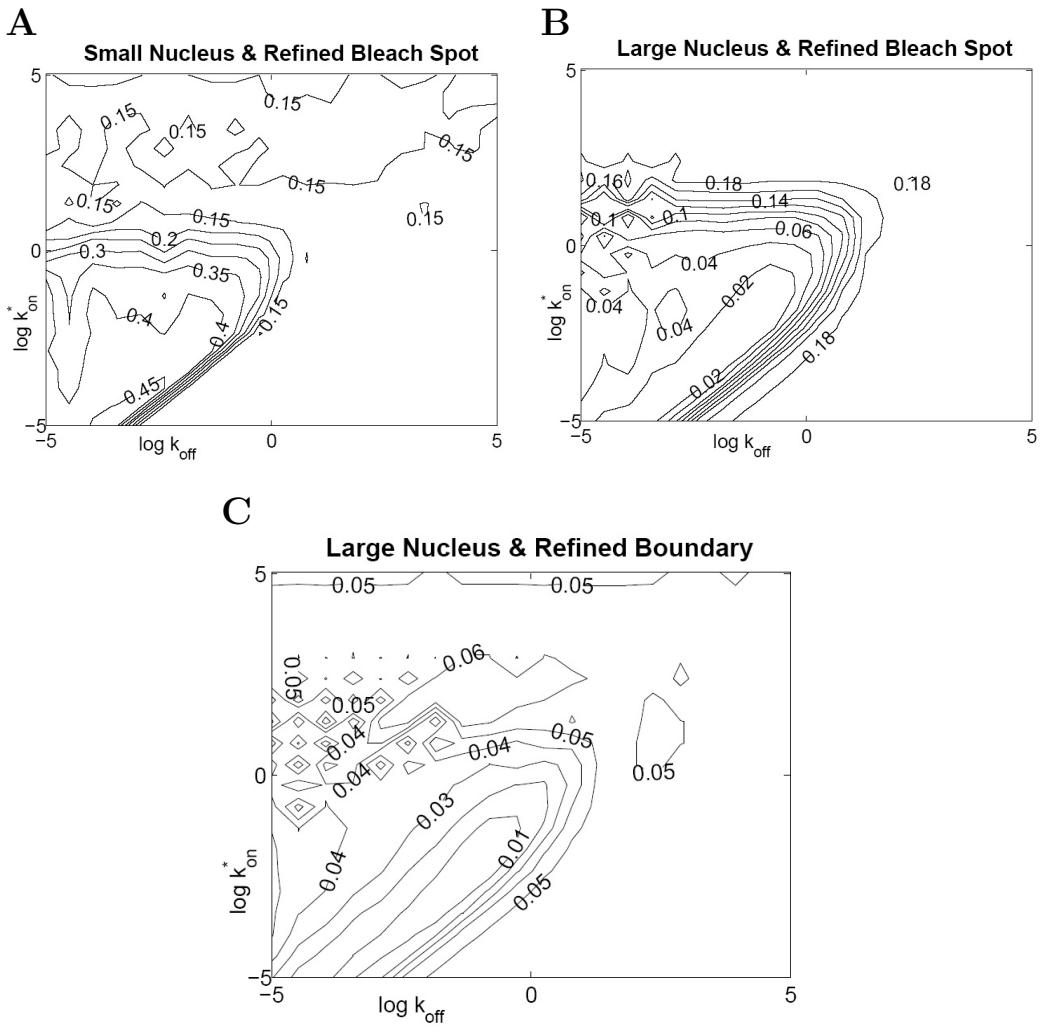

Figure 4.5: ***Sum of the residuals****.* ***A*** *Bleach spot four times refined with a small nucleus (7.5 µm).* ***B*** *Bleach spot four times refined with a large nucleus (50 µm).* ***C*** *Boundary of the bleach spot refined with a large nucleus.*

The refinement of the mesh of the bleach spot improves the quality of the solution immensely for the diffusion and pure-diffusion regime but not for the reaction dominant regime (Figure 4.5). Even the initial mesh produces good results for this model and any further increase of the mesh size barely brings any improvement. This regime show a much bigger sensitivity with respect to the size of the nucleus. An increased nucleus reduces the sum of the residuals obviously (Table 4.5). Thus, the numeric solution can be considered to produce accurate results even with small meshes, the differences to the analytic solution arise because of the bounded nucleus in the numeric model.

4.1.5 Conclusion

In the previous sections I derived some important aspects one should keep in mind if the FEM is used for the numeric solution of FRAP experiments.

The accuracy of the recovery curve shows a strong dependency on the mesh size for some domains in the binding rates parameter space, namely for the diffusion regime, the effective diffusion regime, and the full model regime. In Figure 4.3 the actual influence of the sum of the residuals can be seen for some recovery curves. Two recovery curves with a value for the residuals of 0.66 or even 2.4 are obviously different. For the further simulations I choose a threshold of 0.1 for the sum of the residuals beyond which the curves were different. What follows from the analysis of the influence of the mesh size is that a selective refinement of the bleach spot boundary yields the best results. In Table 4.4 the influence of the number of points on the boundary to the sum of residuals can be seen for a bleach spot of radius $0.5\mu m$. With the above defined threshold the boundary should be described at least with 150 points in order to guarantee the reliability of the numeric solution. The total number of finite elements should not be significantly larger than $3,000$. With meshes of this size the whole parameter space can be investigated within an acceptable time span (see Table 4.5). The reason why this selective refinement strategy delivers the best results can be explained on closer examination of the the photobleaching process and the way FEM solves the underlying differential equations. The bleaching introduces a rapid shift away form the equilibrated concentrations. Directly after the bleaching the concentration gradient of the fluorescent proteins is not only very steep at the bleach spot's boundary but it is even a jump for an uniform bleaching profile. This jump in the concentrations ranges from zero inside the bleach spot to a distinct equilibrated value outside. The accuracy of the numeric solution depends on how good the behavior of the solution in this part of the geometry can be resolved. In the FEM small triangles are needed only in those parts of the computational domain where the function values change

fast. Smaller elements reduce the numeric error that where made in this part of the geometry. The selective refinement of the triangle at the bleach spot's boundary takes this fact into account and enables the resolution of the fast diffusive processes after the photobleaching and thus improves the accuracy of the solution.

The second important observations that follows from the program validation is that the accuracy of the solution for the reaction dominant regime does not mainly depend on the mesh size. Better agreement between the numeric and analytic solution can be obtained by increasing the radius of the nucleus. For this domain the size of the nucleus influences not only the final height of the recovery curve but also the time course of the recovery. This fact has to be considered if the analytic solution is used to describe the FRAP recovery on a bounded domain. The assumption of a larger nucleus is of particular importance for the reaction dominant regime, ignoring this would yield a wrong interpretation of the data.

4.2 Simulation of FRAP experiments

In the first section I have shown that the numeric model with a selective refined mesh at the boundary of the bleach spot yields accurate results. The recovery curve is not only influenced by the underlying biophysical parameters but also by the geometry on which the PDE problem is solved. The analytic solution, however, does not consider different geometries and hence it is of particular interest to know how a change in the experimental setup influences the solution. The numeric model can now be used to assess the influence of changes in the experimental geometry to the recovery curve. Since the magnitude of this influence might depend on the binding rates I used *FrapDomain* again for a comprehensive investigation of the whole parameter space formed by the binding rates. The impact of changes in the experimental geometry can be quantified by comparing the results of the numeric simulation before and after the corresponding change. Since the numeric results can be considered to be correct, differences in the behavior of the recovery are then due to this change and not because of an inaccuracy of the numeric model. For the *reference solution* I used a circular nucleus with a radius of $R_{NS} = 7.5\,\mu m$, the bleaching was done within a concentric bleach spot with a radius of $w = 1\,\mu m$ and a uniform bleaching profile. The diffusion coefficient was set to a value $D_f = 30\,\mu m^2/s$.

During the various simulations with different experimental setups it became obvious that the concept of different domains in the parameter space of the binding rates as described in section 2.3.8 is very suitable for the de-

scription of the results. The sum of residuals had often the same magnitude for a whole regime. This is reasonable because the regimes are chosen based on physical considerations and thus represent groups with similar physical properties. It is therefore likely that the response to a certain change is the same throughout a distinct regime. For a further summarization I will refer to the pure-diffusion regime and the effective-diffusion regime as *diffusive regimes*, since diffusion plays the major role here.

4.2.1 Influence of the nuclear membrane

An important difference between the analytic solution (section 2.3.7) and a real FRAP experiment is the domain on which the recovery process happens. The analytic approach solves the reaction-diffusion equation on an infinite domain, whereas in reality the movement of the proteins is restricted to the nucleus, i.e., a bounded domain. The introduction of the nuclear membrane into the mathematical model yields two important effects. First, the fluorescent pool is restricted to a certain number. Second, the position where the photobleaching is performed influences the rate of fluorescence recovery. The numeric solution calculated in *FrapSim* is also restricted to a user defined geometry. It is therefore a convenient tool to assess the influence of the nuclear membrane to the recovery curve.

Influence on the asymptotic behavior of the recovery

The final height of the recovery curve for a finite sized nucleus depends on the area of the nucleus A_{NS} and of the bleach spot A_{BS}. It can be calculated with Eq. 3.5 together with the radius of the nucleus R_{NS} and the radius of the bleach spot w:

$$F_\infty = \frac{A_{NS} - A_{BS}}{A_{NS}} = \frac{{R_{NS}}^2 - w^2}{{R_{NS}}^2}. \tag{4.1}$$

A second possibility to obtain this value is to simulate the recovery process for a sufficient long time span. The binding rates influence the FRAP recovery times but not the asymptotic value of the recovery curve F_∞. Thus, it is not necessary to consider them for this investigation and I used a numeric model without a binding site. I varied the bleach spot radius w from 0.5 to 3.0 μm and considered the value of the recovery curve at $t = 5\,s$ as the final height of the recovery. This time interval is large enough to guarantee the fluorescence intensity has fully recovered. The FRAP recovery times for $D_f = 30\,\mu m^2/s$ range from $\sim 1-3\,s$ depending on the bleach spot radius.

Table 4.6: Final height of the recovery curve for different bleach spot radii. w is bleach spot radius, F_{eq} the value of the recovery curve at $t = 5\,s$, F_∞ the calculated final height of the recovery curve (Eq. 4.1).

w (μm)	F_{eq}	F_∞
0.5	0.9953	0.9956
1.0	0.9813	0.9822
1.5	0.9578	0.9600
2.0	0.9264	0.9289
2.5	0.8830	0.8889
3.0	0.8347	0.8400

The calculated and simulated values for different bleach spot sizes match to the third decimal place and this degree of agreement is sufficient enough to state that the numeric approach simulates the loss of of fluorescence in an accurate way.

Influence on the rate of fluorescence recovery

To assess the influence of the photobleaching on a bounded domain to the recovery curve I did simulations with different positions of the bleach spot with respect to the nuclear boundary.

Table 4.7: Influence of bleach spot position on the recovery curve. x_{BS} is the displacement of the bleach spot to the center of the nucleus.

$x_{BS}(\mu m)$	Δ_{NS}	Δ_{BS}	N_{bound}	$Resid_{max}$
0	3460	1388	238	-
1	3712	1555	273	0.09
2	3650	1508	256	0.18
3	3936	1566	278	0.43
4	3766	1535	269	0.86
5	3205	1284	216	1.57
6	3965	1660	278	3.12
6.5	3833	1681	309	3.74

I calculated the reference solution with a centered bleach spot ($x_{BS} = 0\,\mu m$). For the following simulations I shifted the bleach spot successively closer towards the boundary by increasing the x-coordinate x_{BS}. For each new position I calculated the recovery curves for the whole parameter space and estimated the sum of the residuals with the reference solution.

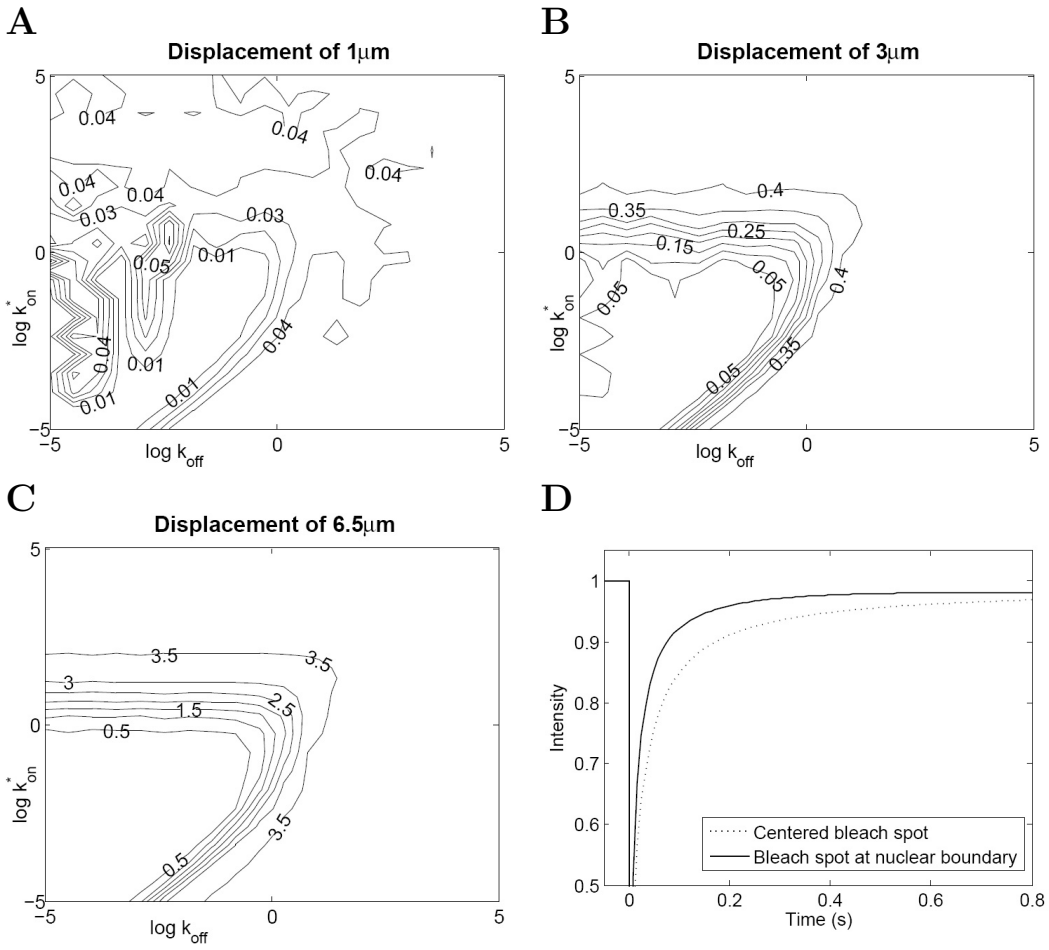

Figure 4.6: ***Influence of the nuclear boundary****. Reference solution with centered bleach spot.* ***A*** *Sum of residuals with a bleach spot positioned at* $x_{BS} = 1\,\mu m$. ***B*** *Bleach spot at* $x_{BS} = 3\,\mu m$. ***C*** *Sum of residual with the bleach spot placed at the nuclear boundary* ($x_{BS} = 6.5\,\mu m$). ***D*** *Recovery curve for pure diffusion regime* ($k^*_{on} = 10^{-3}s^{-1}$, $k_{off} = 10^3 s^{-1}$) *and different bleach spot positions. Sum of residuals between the curves is 3.7.*

The rate of fluorescence recovery shows a strong dependency on the bleach spot position for those regimes where the diffusion plays at least a minor role, i.e., for the full model regime and the diffusive regimes (Figure 4.6).

By placing the bleach spot closer to the boundary less unbleached proteins have the possibility to move inside. This reduced amount of fluorescent proteins yields a slower fluorescence recovery. Thus, it can be stated that for systems where the recovery process depends on the diffusion process a bleaching close to the nuclear boundary yields a slower rate of fluorescence recovery. For the reaction dominant regime, on the other hand, the diffusion is much faster than the binding events. The rate of fluorescence recovery is, thus, only governed by the binding interactions in the bleach spot. The bleach spot position influences the availability of freely diffusing proteins and has therefore no influence on the recovery curve for the reaction dominant regime.

Misinterpretation of experimental data

The position of the bleach spot has the greatest impact on the the recovery curve for the diffusive regimes. Here the recovery slows significantly down. For a more detailed investigation I choose a numeric model with coefficient of $D_f = 30\,\mu m^2/s$ and without a binding site. I calculated the recovery curves for the same geometries as before. Then I treated the simulated recovery curves like experimental data and used the *FrapFit* environment to estimate the diffusion coefficient for each curve. The deviation between the estimated and simulated diffusion coefficient can be expressed with the relative error, which is defined as the difference between the simulated and the estimated value divided by the simulated value.

Table 4.8: Estimated diffusion coefficient for different bleach spot positions. Sum of residuals are calculated between the analytic solution with the estimated diffusion coefficient $\mathrm{D_{f,est}}$ *and the simulated data with* $D_f = 30\,\mu m^2/s$.

$\mathrm{x_{BS}}(\mu\mathrm{m})$	$\mathrm{D_{f,est}}(\mu\mathrm{m}^2/\mathrm{s})$	Residuals	Error
0	29.15	0.427	2.8%
1	29.17	0.465	2.7%
2	28.92	0.597	3.6%
3	28.36	0.816	5.5%
4	27.27	1.149	9.1%
5	24.90	1.407	17.0%
6	19.07	1.670	36.4%
6.5	14.66	1.055	51.1%

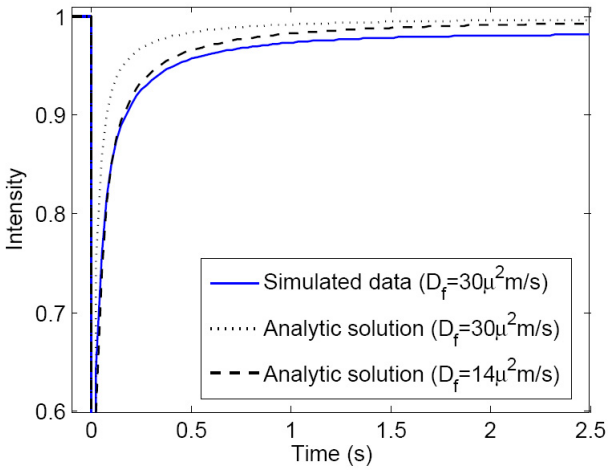

Figure 4.7: ***Recovery curves****. The bleaching was performed at the nuclear boundary and slows down the recovery process. The reduced diffusion coefficient of the fitted solution lowers the curve which yields a better fit.*

The analytic solution is defined for an infinite nucleus and does not consider the nuclear boundary. A recovery curve calculated with this approach will lie above the recovery curve obtained from a numeric simulation with the same biophysical parameters simply because it does not consider the slower recovery due to the bleach spot position (see Figure 4.7). A lowering of the recovery curve in the analytic solution is only possible by decreasing the diffusion coefficient. This happens if the experimental data is fitted with the analytic solution in order to estimate the diffusion coefficient or the binding rates. The fitting routine compensates for the lowered recovery curve of the experimental data by using a smaller value for the diffusion coefficient. This results in a underestimation of the diffusion coefficient (Table 4.8).

4.2.2 Influence of the bleached geometry

Photobleaching experiments performed on a CLSM are not restricted to circular bleaching geometries, it is possible to bleach virtually any pattern. The amount of photobleached molecules depends only on the bleached area (Eq. 3.5) if homogeneously distributed fluorescent molecules can be assumed. Bleach spots with different geometries but the same area thus yield the same final height of the recovery curve. The open question is how the shape of the bleach spot influences the rate of fluorescence recovery. Usually bleaching is either performed within a circular bleach spot or within a so called bleach-stripe, i.e., rectangular bleaching geometries. An analytic solution for bleach stripes is derived in [8]. In this model the nucleus is assumed to be

rectangular and the bleaching is performed on a narrow band over the whole nucleus. Since this model is restricted to a certain geometry it is not suitable to describe rather general experimental setups. *FrapSim* provides with its ability to define arbitrary bleach spots a convenient possibility to investigate the influence of different bleaching geometries.

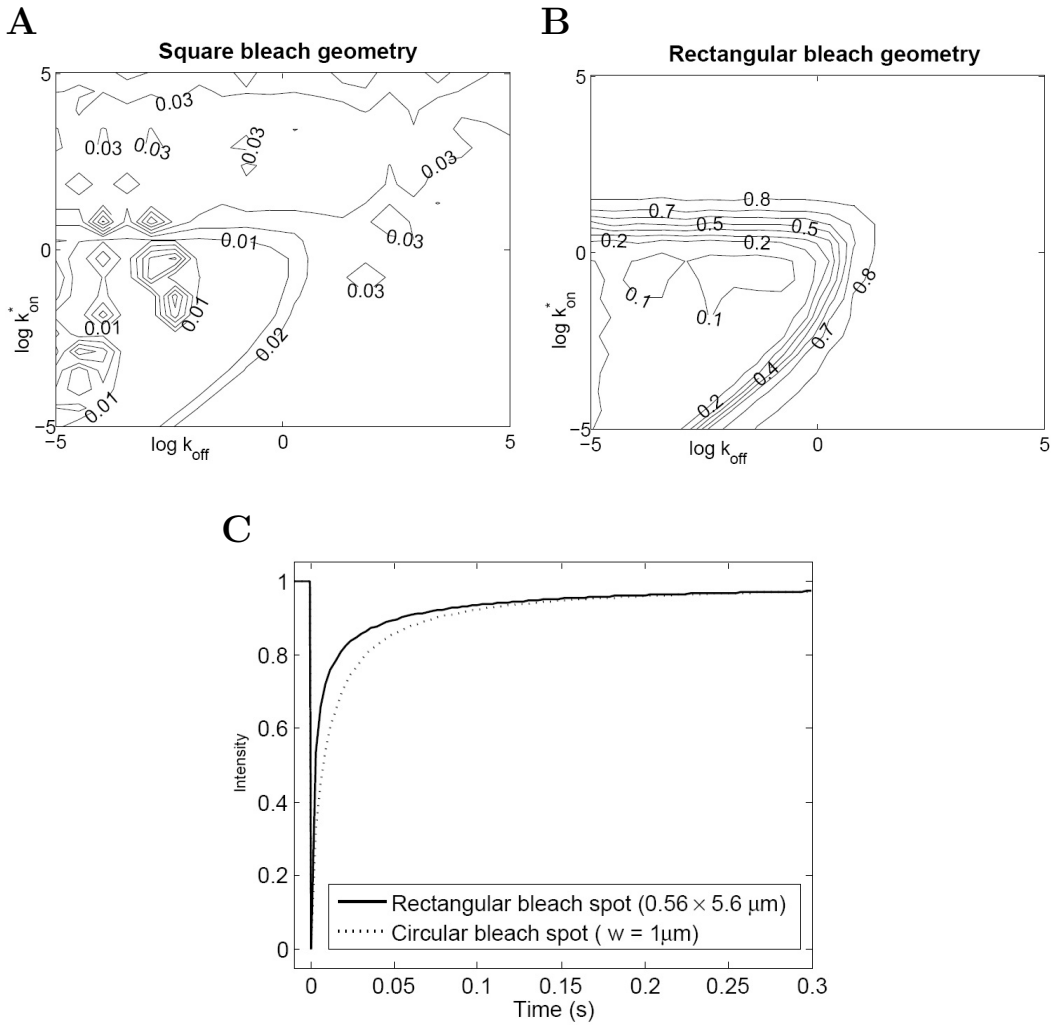

Figure 4.8: ***Influence of the bleach spot geometry****. Reference solution with concentric bleach spot and nucleus.* ***A*** *Sum of residuals for a square bleach pattern (*$1.77 \times 1.77\,\mu m$*).* ***B*** *Sum of residuals for a narrow rectangular bleach pattern (*$0.56 \times 5.6\,\mu m$*).* ***C*** *Recovery curve for pure diffusion regime (*$k^*_{on} = 10^{-3}\,s^{-1}$*,* $k_{off} = 10^3\,s^{-1}$*) and different bleach spot geometries. Sum of residuals between the curves is 0.8.*

To assess the influence of the bleached geometry on the recovery curve I simulated FRAP experiments with different rectangular bleach patterns. I used the numeric solution with the centered bleach spot of the previous section as reference solution for the calculation of the residuals. Since the radius of the bleach spot is $w = 1\,\mu m$, the bleached area is $A_{BS} = w^2\pi = \pi\,\mu m^2$.

Table 4.9: Bleaching of different rectangular bleach spots

Side lengths (μm)		N_{bound}	$Resid_{min}$	$Resid_{max}$
1.77	1.77	258	0.000	0.072
1.02	3.07	231	0.029	0.422
0.56	5.60	312	0.032	0.876

I defined the side length of the rectangles so that the area of the resulting rectangle was $\sim 3.14\,\mu m^2$. Hence, only the rate of fluorescence recovery may change but not the asymptotic behavior of the recovery curve. I positioned the rectangles at the center of the nucleus in order to minimize the influence of the nuclear boundary.

The differences between the square bleach geometry and the circular are very small for the whole parameter space and are almost negligible. Even the maximum value for the sum of the residuals of 0.072 (Table 4.9) is so small that the two curves are not distinguishable from each other with the naked eye. These results suggest that there is no remarkable difference between bleaching a circular pattern or a square pattern as far as the recovery curve is concerned. This changes if rectangular patterns are bleached. For the diffusive regime and the full model regime the rate of recovery is the faster, the narrower the bleach stripe. This is evident, since for a narrow rectangle the mean path length for a unbleached molecule to move inside the bleached area is smaller than, e.g., for a square. Thus, the fluorescence recovery gets faster with a narrower bleach stripe for the regimes for which the diffusion is important. Whereas for the reaction dominant regime the rate of recovery depends only on the binding events and the shape of the bleached area has, thus, no influence on the recovery curve.

4.2.3 Influence of the nucleolus

The nucleoli are the nuclear compartments where the ribosomes are produced. They differ in number and shape from nucleus to nucleus. For the

implementation in *FrapSim* they are considered to be regions within the nucleus where only diffusion occurs. Therefore, the proteins undergo binding events in the nucleoplasm but not in the nucleolus.

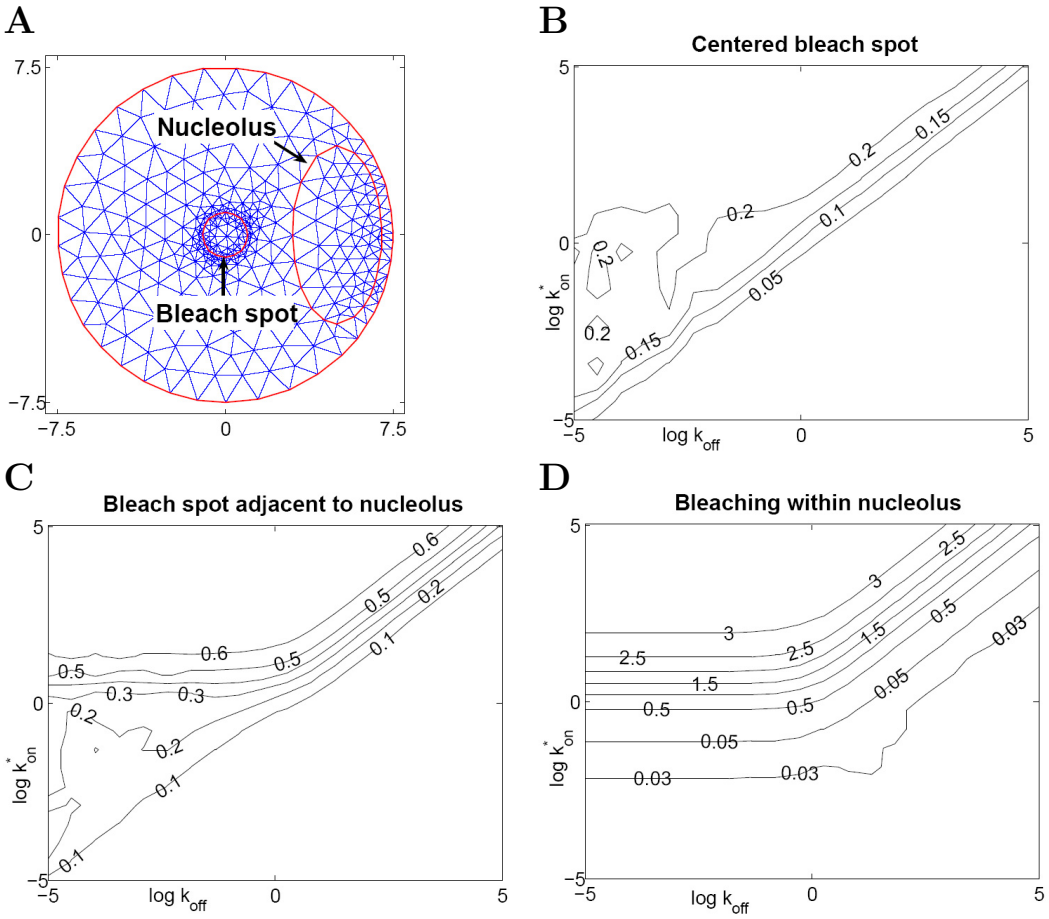

Figure 4.9: ***Influence of the nucleolus****. Reference solution with same geometry but without nucleolus.* ***A*** *Geometry with the bleach spot, the nucleolus, and the mesh with refined bleach spot boundary.* ***B*** *Sum of residuals for centered bleach spot.* ***C*** *Sum of residuals for bleach spot adjacent to the nucleolus.* ***D*** *Sum of residuals for bleaching within the nucleolus.*

For simplicity I used the same model as described above and added only one elliptic nucleolus with center coordinates $x = 5\,\mu m$ and $y = 0\,\mu m$, and semi-axis $s_x = 2\,\mu m$ and $s_y = 4\,\mu m$. The first calculation was performed with a centered bleach spot ($x_{BS} = 0\,\mu m$). For the second calculation I positioned the bleach spot adjacent to the boundary of the nucleolus ($x_{BS} = 2\,\mu m$). I calculated the sum of the residuals with the solutions obtained with the same geometries but without the nucleolus (section 4.2.1).

Table 4.10: Influence of the nucleolus on the recovery curve

$x_{BS}(\mu m)$	N_{bound}	$Resid_{min}$	$Resid_{max}$
0	246	0.001	0.245
2	265	0.002	0.667
5	235	0.023	3.331

I simulated a bleaching within the nucleolus with the last run, i.e., the bleach spot was defined to be concentric with the nucleolus ($x_{BS} = 5\,\mu m$). In this case the bleaching is performed in small area without any binding sites. The recovery process is thus mainly governed by the free diffusing proteins within the nucleolus. The binding site play a minor role for the fluorescence recovery and the timescale of the simulation is mainly determined by the diffusion coefficient and the bleach spot radius. Thus, I choose a recovery time of $t = 1.5\,s$ for the calculation of the numeric solution for the whole parameter space with *FrapDomain*. I calculated the reference solution with the same position of the bleach spot but without the nucleolus and any binding site.

The nucleolus influenced the recovery curves for the effective diffusion regime most. I choose one pair of binding rates describing this behavior ($(k^*_{on} = 10^4\,s^{-1}$, $k_{off} = 1\,s^{-1}$) and calculated recovery curves for a bleach spot at $x_{BS} = 2\,\mu m$ and $x_{BS} = 5\,\mu m$ with two different approaches. I calculated the recovery curve for the numeric model with the binding site first with the nucleolus and second without the nucleolus. As a second approach I calculated the effective diffusion coefficient D_{eff} with Eq. 2.29

$$D_{eff} = \frac{D_f}{(1 + (k^*_{on}/k_{off}))} = \frac{30}{1 + 10^4} = 0.003\,\mu m^2/s, \tag{4.2}$$

The effective diffusion coefficient describes the slower movement of the proteins outside the nucleolus. Inside the nucleolus the diffusion coefficient of $D_f = 30\,\mu m^2/s$ is still valid. With D_{eff} and the original diffusion coefficient D_f the system can be described without the bound state. I solved this model again first with the nucleolus and second without the nucleolus.

Bleaching regions adjacent to the nucleolus

The results for different bleaching position are summarized in Figure 4.9. It is obvious that the nucleolus influences the rate of fluorescence recovery especially for the effective diffusion regime. Here the recovery gets the slower,

A

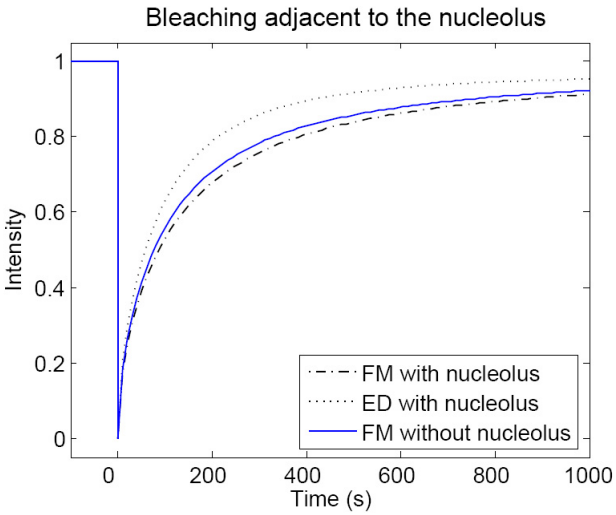

B

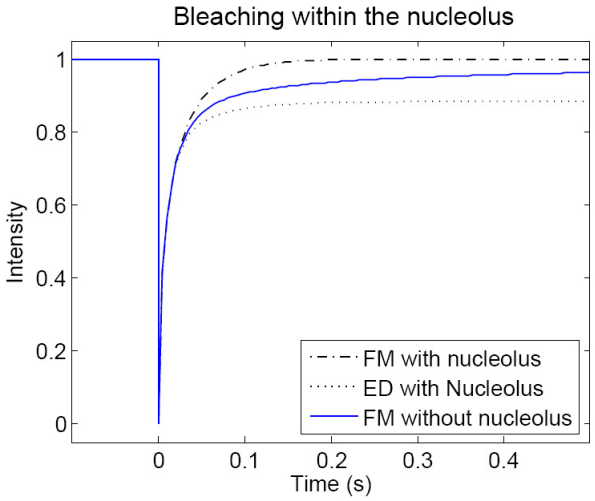

Figure 4.10: ***Recovery curves*** *for the effective diffusion regime ($(k^*_{on} = 10^4\, s^{-1},\ k_{off} = 1\, s^{-1})$. The dash-dotted curve (FM) was calculated with the nucleolus and the binding site outside the nucleolus. The dotted curve (ED) was calculated with the effective diffusion coefficient $D_f = 0.003\,\mu m^2/s$ outside the nucleolus and a diffusion coefficient $D_f = 30\,\mu m^2/s$ within the nucleolus.* ***A*** *Bleaching adjacent to the nucleolus ($x_{BS} = 2\,\mu m$) Reference solution (blue line) calculated with binding site and no nucleolus.* ***B*** *Bleaching within the nucleolus ($x_{BS} = 5\,\mu m$) Reference solution (blue line) calculated without nucleolus and without binding site.*

the closer the bleaching is performed to the nucleolus (Figure 4.10A). This results is astonishing at first sight since the recovery gets even faster if the system is described with an effective diffusion coefficient (Section 2.3.8).

The main characteristic of the *effective diffusion regime* is that the initial reaction-diffusion problem can be described with a simple diffusion equation and a new diffusion coefficient D_{eff}. This so called effective diffusion coefficient takes the slowed movement of the proteins due to binding events into account. I used the initial coefficient of $D_f = 30\,\mu m^2/s$ for the nucleolus and the effective diffusion coefficient $D_{eff} = 0.003\,\mu m^2/s$ for the nucleoplasm, i.e., the rest of the nucleus. Now the system is described just by the free diffusing proteins, but they are moving much faster in the nucleolus than in the nucleoplasm. The photobleaching introduces a concentration gradient and the diffusion leads to a directed flow of proteins. Since $D_{eff} \ll D_f$ the time scale of protein movement within the nucleolus is so fast that concentration gradients at its boundary are instantaneously compensated and a local steady state can be assumed throughout the nucleolus. The proteins within the nucleolus react much faster to the concentration gradients introduced from the photobleaching and therefore yield a faster recovery of the fluorescence intensity.

The *full model*, however, describes the system only with one diffusion coefficient for the whole nucleus but considers explicitly the binding site in the nucleoplasm. The corresponding binding rates can not only be used to calculate the effective diffusion coefficient, but also to calculate the ratio of the concentration of bound to free proteins with Eq. 2.18:

$$\frac{C_{eq}}{F_{eq}} = \frac{k^*_{on}}{k_{off}} = 10^4. \tag{4.3}$$

For the reaction dominant regime the pool of bound proteins is much larger than the pool of the free proteins. The fluorescence recovery arises from both the bound fluorescent proteins and the free fluorescent proteins. The latter play a negligible role because of their minor concentration. Thus, the freely diffusing proteins of the nucleolus have no remarkable influence. Furthermore, it even seems that the lack of bound proteins due to the nucleolus slows down the recovery process.

For the other regimes there is no remarkable influence of the nucleolus on the recover curve. This is evident for the pure-diffusion regime because the bindings in the nucleoplasm are very weak and therefore there is no actual difference between the nucleoplasm and the nucleolus. For the reaction dominant regime the recovery depends only on the binding events within the bleach spot. A region with a different diffusive behavior like the nucleolus has anyway no influence on the recovery.

Bleaching within the nucleolus

Photobleaching can also be performed within the nucleolus, i.e., only the freely diffusing proteins within the nucleolus contribute to the recovery of fluorescence intensity. The protein dynamics can again be simulated with the full model or the effective diffusion model. With the first approach the recovery gets faster, whereas with the second approach the recovery gets slower (Figure 4.10).

The effective diffusion model states that the proteins in the nucleoplasm diffuse much slower than the one in the nucleolus because of the different diffusion coefficients. The recovery process can be described with two phases which occur on different timescales. First, the free proteins within the nucleolus re-equilibrate and achieve a local steady state. The timescale of this process is determined by the diffusion coefficient D_f and is on the order of $\sim 1\,s$. The height of the recovery curve due to this process can be calculated with the ratio of the unbleached area of the nucleolus to the total area of the nucleolus[1] with Eq. 3.5:

$$F_\infty = \frac{A_{NS} - A_{BS}}{A_{NS}} = 0.875. \tag{4.4}$$

The compensation of the resulting concentration gradient between nucleolus and nucleoplasm happens on the much slower timescale of the effective diffusion coefficient D_{eff} ($\sim 1000\,s$).

This is different if the full model is used to describe the experiment. The fluorescence recovery arises again from the free proteins within the nucleolus, but outside the nucleolus the proteins interact with a binding site and exist in a free and a bound state. At the boundary of the nucleolus is hence a very large pool of bound proteins. These bound proteins released after an average binding time of $\tau_b = 1/k_{off} = 1\,s$ (section 2.3.2), a small portion releases even earlier since this binding time is only an average value. The released proteins may now diffuse into the nucleolus and contribute here to the recovery of fluorescence intensity. The rate of fluorescent recovery gets faster if the nucleolus is surrounded with such bound proteins. It seems that the number of bound proteins that dissociate from their binding sites and move inside the nucleolus is larger as if the nucleolus is surrounded only with free proteins that diffuse inside.

[1] Area of the nucleolus $A_{NS} = \pi ab \approx 25\,\mu m^2$

4.2.4 Conclusion

I have developed a convenient tools for accurate numeric simulations of FRAP experiments with general experimental geometries. The graphical user interface enables even users which are not familiar with the Finite Element Method and its implementation to work with these tools.

The results from the previous sections show that changes in the geometry of the experimental setup of a FRAP experiment may influence the resulting recovery curves. This influence is not the same for all possible binding rates, but can be formulated and motivated for the different regimes. In general it can be stated that the recovery curves did not change quantitatively, i.e., the recovery curves showed no new characteristics but the recovery process gets faster or slower.

For the *reaction dominant regime* the recovery curve is mainly influenced by the size of the bleach spot compared to the nucleus. Placing the bleach spot near the nuclear boundary or different bleaching geometry do not influence the rate of fluorescent recovery.

The rate of fluorescence for the *diffusive regimes* react sensitive to changes in the geometry since these changes influence the possibility of the proteins to diffuse. The recovery curves for the effective diffusion regime is in addition influenced by the nucleolus, i.e., a structure where no binding sites are present. During the analysis it became apparent that the simplified description with the effective diffusion coefficient delivers only correct results if this coefficient is valid for the whole geometry. For composite regions the full model must be used to describe the protein dynamics properly.

The *full model regime* can not be described with one of the simplified approaches alone. The fluorescence recovery is influenced by both the diffusion and the binding events. The exact values of the binding rates determine which of the two processes is more important. The response of the recovery curve to changed geometries shows, thus, a transition from the rather reaction dominant behavior to the diffusive behavior.

4.3 Outlook and future work

The mathematical model describes the protein dynamics during a FRAP experiments with a system of reaction-diffusion equations. It is possible to simulate FRAP experiments with the *FrapSim* and *FrapDomain* environment for very general experimental setups. The numeric model predicts a sensitivity of the recovery curves towards changes of the experimental geometry. It would be of particular interest to compare these theoretic obtained results

with data from real experiments. This would allow further assessments of the biological model.

The mesh that is necessary to guarantee that the numeric solution is accurate is very large. This results in long computation times if the whole parameter space of the binding rates is explored. There exist other approaches for FEM to solve the problem of the inaccuracy of the diffusion domain beneath the selective mesh refinement strategies. In the *streamline diffusion method* an artificial diffusion term is introduced which corrects some of the errors [19]. An implementation of a comparable method would enable a solution with smaller meshes sizes and hence reduce the computation time significantly.

Appendix A

FrapSim

A.1 System requirements

FrapSim was developed and tested with Matlab 7.0 running on Windows XP. All simulations were performed on a PC system with an AMD Athlon Processor 1800 with 256 MB RAM.

A.2 Classes in *FrapSim*

Table A.1: Visual classes used in FrapSim.

Class name	Brief description
FrapSim	The overall graphical user interface.
GUIgeometryElliptic	Definition of elliptic geometries.
GUIgeometryRectangular	Definition of rectangular geometries.
GUIdiffusioncoefficient	GUI for editing the diffusion coefficient.
GUIbindingrates	GUI for editing the binding rates.
GUIfrapDomain	Open the GUI of *FrapDomain*
GUIfrapDomain	Open the GUI of *FrapSim*
GUIshowequation	Shows the reaction-diffusion equation.
GUIflip	GUI for editing the the number of bleach cycles during FLIP.
GUItimeresolution	GUI for editing the time resolution.
GUIanimation	GUI for the animation of the solution.
GUIdefineCrossSection	GUI for defining a cross-section through the nucleus.

Table A.2: Auxiliary classes used in FrapSim.

Class name	Brief description
activategaussian	Gaussian photoactivation within the bleach spot.
activateuniform	Uniform photoactivation within the bleach spot.
bleachgaussian	Gaussian photobleaching within the bleach spot.
bleachuniform	Uniform photobleaching within the bleach spot.
boundarycondition	Calculate the boundary matrix with no-flux bc's.
calcrecovery	Calculate the values for the recovery curve.
concentrationequ.	Calculate equilibrated concentrations.
dimensionsystem	Return the dimension of the system.
export	Export parts of a project the workspace.
frapanalyticOne	Analytic solution for one binding state.
frapanalyticTwo	Analytic solution for two binding states.
frapOneLT	Laplace transform for one-binding-state model.
frapTwoLT	Laplace transform for two-binding-state model.
geometrydelete	Delete a graphical object.
geometryedit	Edit object with rectangular or elliptic geometry.
geometryelliptic	Create or edit object with elliptic geometry.
geometryrectangular	Create or edit object with rectangular geometry.
getcolumn	Return column number of a geometric object.
importgeometry	Import CSG model variables from workspace.
invlap	Numerical inverse Laplace transformation.
isobjectdefined	Return column number of a geometric object.
pdecoefficients	Calculate the PDE coefficients for the problem.
pdegplotMod	Matlab function pdeplot with user defined color.
plotmesh	Plot the triangular mesh.
plotgeometry	Plot the geometry of the simulation.
plotrecoverycurve	Plot the recovery curve.
projectnew	Initiate all variables for a new project.
projectload	Load project data from a file.
projectsave	Save project data to a file.
solveflip	Calculate the solution for a FLIP experiment.
subdomainlist	Return all subdomains of one solid object.

A.3 Workflow in *FrapSim*

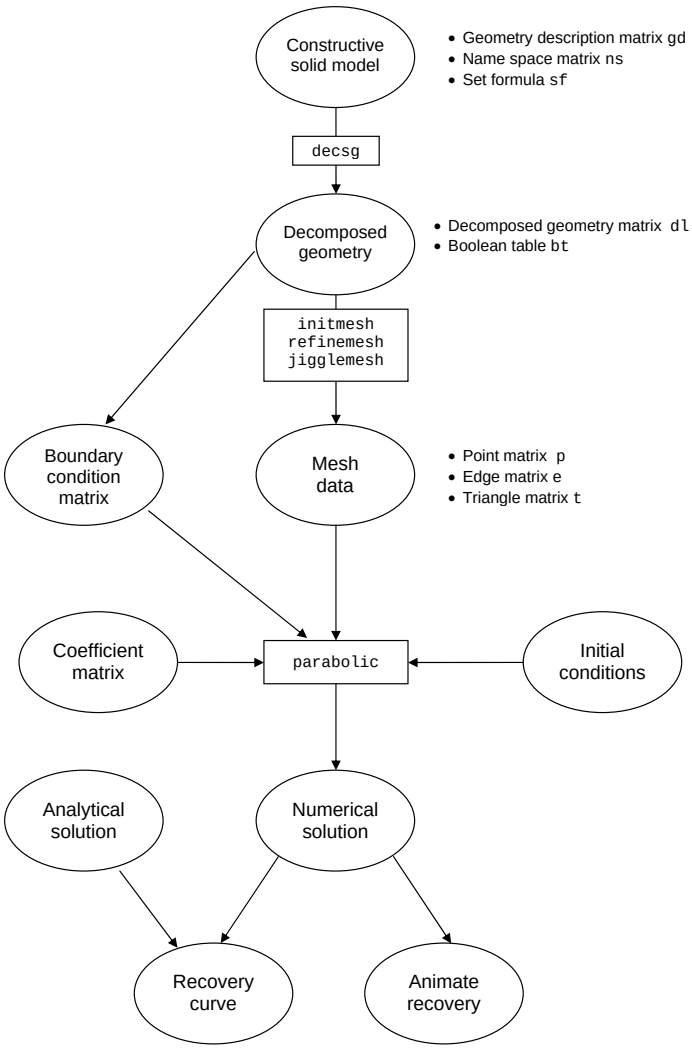

Figure A.1: Workflow in FrapSim

Fig. A.1 shows a graphical representation of the typical workflow for the solution of a PDE problem with *FrapSim*. The rectangles are functions, and ellipses are data represented by matrices.

A.4 PDE coefficients in *FrapSim*

The reaction-diffusion equation for the one binding state described by Eq. 2.17 can be rewritten in matrix form:

$$\begin{pmatrix} 1 & 0 \\ 0 & 1 \end{pmatrix} \frac{\partial}{\partial t}\vec{u} - \begin{pmatrix} D_f & 0 \\ 0 & 0 \end{pmatrix} \nabla^2\vec{u} - \begin{pmatrix} -k_{1on} & k_{1off} \\ k_{1on} & -k_{1off} \end{pmatrix} \vec{u} = 0. \quad \text{(A.1)}$$

The solution vector $\vec{u}$ of the independent variables describes the concentration of the free proteins f_p and the concentrations of the bound proteins c_1:

$$\vec{u} = \begin{pmatrix} f_p \\ c_1 \end{pmatrix}. \quad \text{(A.2)}$$

The parabolic partial differential equation that can be solved in Matlab with the FEM can be written in the form:

$$\underline{d}\frac{\partial u}{\partial t} - \nabla \cdot (\underline{c} \otimes \nabla u) + \underline{a}\, u = f \text{ on } \Omega. \quad \text{(A.3)}$$

By comparing Eq. A.1 and Eq. A.3 the *Matlab coefficient matrices* can be estimated. To avoid confusion *Matlab coefficient matrices* are written with `typewriter` font, the matrices from Eq. A.1 in *italics*. Some matrices in Eq. A.1 have mainly zeros as elements. To ease the definition Matlab uses special formats to code the coefficient matrices:

1. The elements of each matrix in Eq. A.3 are stored row-wise in the coefficient matrix, i.e., each row in coefficient matrix corresponds to one single element.

2. The coefficients are defined for each subdomain, i.e., one column of the coefficient matrix holds the values for the corresponding subdomain. The values for each subdomains are separated by exclamation marks.

For more details on the coefficient data structures, see the reference page for the Matlab function `assempde`.

Simple example

To get an understanding of how the coefficient matrices are defined they are derived for a simple system. The geometry consists of a nucleus and one binding site with a separate geometry. The decomposed geometry consists of four subdomains, the binding site is defined in subdomains 2 and 4. On the

left hand side the coefficient matrices are shown as they are stored in Matlab, on the right hand side the corresponding coded matrices are indicated (`c`(i) corresponds to the i^{th} row of `c`).

Vector f

The number of rows in **f** determines the dimension N of the system. The independent variables describe the concentration of the free proteins and of the bound proteins. The dimension of the system is thus 2. This is indicated by `f` having two rows. As f does not appear in Eq. A.1 all elements are zero:

$$\texttt{f} = \begin{bmatrix} !0!0!0!0!0! \\ !0!0!0!0!0! \end{bmatrix} \Leftrightarrow \begin{array}{|c|} \hline \texttt{f}(1) \\ \hline \texttt{f}(2) \\ \hline \end{array}$$

Matrix d

The Matrix d has ones on the diagonal and zero everywhere. This is true for every part of the geometry, i.e., for all subdomains. The diagonal matrix d is coded in Matlab by the definition of a single row for the coefficient matrix `d`.

$$\texttt{d} = [!1!1!1!1!1!] \Leftrightarrow \begin{array}{|c|c|} \hline \texttt{d}(1) & 0 \\ \hline 0 & \texttt{d}(1) \\ \hline \end{array}$$

Matrix a

The matrix a holds the binding rates. The restriction of the binding site to subdomains 2 and 4 is done with this matrix. In the matrix `a` the binding rates are assigned to subdomain 2 and 4, zeros are assigned to the subdomains 1 and 3.

$$\texttt{a} = \begin{bmatrix} !0!k_{on} & !0!k_{on} & ! \\ !0!-k_{on} & !0!-k_{on} & ! \\ !0!-k_{off} & !0!-k_{off} & ! \\ !0!k_{off} & !0!k_{off} & ! \end{bmatrix} \Leftrightarrow \begin{array}{|c|c|} \hline \texttt{a}(1) & \texttt{a}(3) \\ \hline \texttt{a}(2) & \texttt{a}(4) \\ \hline \end{array}$$

Tensor c

Tensor `c` holds the diffusion coefficient D_f which is only assigned to the variable that describes the concentration of the free proteins. The coding of `c` is more complicated, because it is in the most general case a $N \times N \times 2 \times 2$ tensor.

$$\texttt{c} = \begin{bmatrix} !D_f & !D_f & !D_f & !D_f & ! \\ !0 & !0 & !0 & !0 & ! \\ !D_f & !D_f & !D_f & !D_f & ! \\ !0 & !0 & !0 & !0 & ! \\ !0 & !0 & !0 & !0 & ! \\ !0 & !0 & !0 & !0 & ! \end{bmatrix} \Leftrightarrow \begin{array}{|c|c|c|c|} \hline \texttt{c}(1) & \texttt{c}(2) & 0 & 0 \\ \hline \texttt{c}(2) & \texttt{c}(3) & 0 & 0 \\ \hline 0 & 0 & \texttt{c}(4) & \texttt{c}(5) \\ \hline 0 & 0 & \texttt{c}(5) & \texttt{c}(6) \\ \hline \end{array}$$

Bibliography

[1] G. Adam, P. Läuger, and G. Stark. *Physikalische Chemie und Biophysik*. Springer, Berlin, 2003.

[2] William F. Ames. *Numerical methods for partial differential equations*. Academic Press, Inc., 1977.

[3] D. Axelrod, D.E. Koppel, J. Schlessinger, E. Elson, and W.W. Webb. Mobility measurement by analysis of fluorescence photobleaching recovery kinetics. *Biophys. J.*, 16(9):1055–1069, 1976.

[4] J.C.G. Blonk, A. Don, H. Van Aalst, and J.J. Birmingham. Fluorescence photobleaching recovery in the confocal scanning light microscope. *Journal of Microscopy*, 169:363–374, 1992.

[5] Kevin Braeckmans et al. Three-Dimensional Fluorescence Recovery after Photobleaching with the Confocal Scanning Laser Microscope. *Biophys. J.*, 85(4):2240–2252, 2003.

[6] Jose Braga, Joana M.P. Desterro, and Maria Carmo-Fonseca. Intracellular Macromolecular Mobility Measured by Fluorescence Recovery after Photobleaching with Confocal Laser Scanning Microscopes. *Mol. Biol. Cell*, 15(10):4749–4760, 2004.

[7] Edward B. Brown, En Shinn Wu, Warren Zipfel, and Watt W. Webb. Measurement of Molecular Diffusion in Solution by Multiphoton Fluorescence Photobleaching Recovery. *Biophys. J.*, 77(5):2837–2849, 1999.

[8] G. Carrero, E. Crawford, M.J. Hendzel, and G. De Vries. Characterizing Fluorescence Recovery Curves for Nuclear Proteins Undergoing Binding Events. *Bulletin of Mathematical Biology*, 66:1515–1545, 2004.

[9] G. Carrero, E. Crawford, J. Th'ng, G. De Vries, and M.J. Hendzel. Quantification of protein-protein and protein-dna interactions in vivo using fluorescence recovery after photobleaching. *Methods Enzymol*, 375:415–442, 2004.

[10] G. Carrero, D. McDonald, E. Crawford, G. De Vries, and M.J. Hendzel. Using FRAP and mathematical modeling to determine the in vivo kinetics of nuclear proteins. *Methods*, 29:14–28, 2003.

[11] H. S. Carslaw and J.C. Jaeger. *Conduction of Heat in Solids*, chapter The Laplace transformation: problems on the cylinder and sphere, pages 345–347. Oxford University Press, New York, 1959.

[12] J. Crank. *The mathematics of diffusion*. Oxford University Press, London, 1975.

[13] P.S. Dittrich and P. Schwille. Photobleaching and stabilization of fluorophores used for single-molecule analysis with one- and two-photon excitation. *Appl. Phys.*, B 73:829–837, 2001.

[14] Mirsolav Dundr and Tom Misteli. Functional architecture in the cell nucleus. *Biochem. J.*, 356:297–310, 2001.

[15] Inc. Farlex. Thefreedictionary.com. http://encyclopedia.thefreedictionary.com
14th June 2005

[16] Griekspoor, Alexander and Groothuis, Tom. Fast Recovery - Fluorescence Recovery after Photobleaching. http://www.mekentosj.com/science/frap/
14th June 2005

[17] Gordon L. Hager, Cem Elbi, and Matthias Becker. Protein dynamics in the nuclear compartment. *Current Opinion in Genetics & Development*, 12:137–141, 2002.

[18] K. J. Hollenbeck. INVLAP.M: A matlab function for numerical inversion of Laplace transforms by the de Hoog algorithm, 1998. http://www.mathtools.net/files/net/invlap.zip
14th June 2005

[19] Claes Johnson. *Numerical solution of partial differential equations by the finite element method*. Cambridge University Press, 1987.

[20] Jennifer Lippincott-Schwartz et al. Photobleaching and photoactivation: following protein dynamics in living cells. *Nature Cell Biology*, 5:7–14, 2003.

[21] Jennifer Lippincott-Schwartz and George H. Patterson. Development and use of fluorescent protein markers in living cells. *Science*, 300:89–91, 2003.

[22] Jennifer Lippincott-Schwartz, Erik Snapp, and Anne Kenworthy. Studying proteins dynamics in living cells. *Nature Cell Biology Reviews*, 2:444–456, 2001.

[23] Kevin W. Mattison, Ulf Nobbmann, and Dave Dolak. The role of the hydrodynamic radius in biomolecular characterization. *American Biotechnology Laboratory*, pages 66–67, 2001.

[24] James G. McNally, Waltraud G. Müller, Dawn Walker, Ronald Wolford, and Gordon L. Hager. The Glucocorticoid Receptor: Rapid Exchange with Regulatory Sites in Living Cells. *Science*, 287(5456):1262–1265, 2000.

[25] Tom Misteli. Protein dynamics: Implications for nuclear architecture and gene expression. *Science*, 291:843–847, 2001.

[26] Molecular Expressions^{TM}. Exploring the World of Optics and Microscopy. http://micro.magnet.fsu.edu/index.html
14th June 2005

[27] Thoru Pederson. Diffusional protein transport within the nucleus: a message in the medium. *Nature Cell Biology*, 2:73–74, 2000.

[28] Robert D. Phair and Tom Misteli. High mobility of proteins in the mammalian cell nucleus. *Nature*, 404:604 – 609, 2000.

[29] Robert D. Phair and Tom Misteli. Kinetic modelling approaches to in vivo imaging. *Nature Reviews Molecular Cell Biology*, 2:898–907, 2001.

[30] Eric A.J. Reits and Jacques J. Neefjes. From fixed to frap: measuring protein mobility in living cells. *Nature Cell Biology*, 3:145–147, 2001.

[31] Oliver Scholz, Anja Thiel, Wolfgang Hillen, and Michael Niederweis. Quantitative analysis of gene expression with an improved green fluorescent protein. *Eur. J. Biochem.*, 267(6):1565–1570, 2000.

[32] Brian L. Sprague, Robert L. Pego, Diana A. Stavreva, and James G. McNally. Analysis of Binding Reactions by Fluorescence Recovery after Photobleaching. *Biophys. J.*, 86(6):3473–3495, 2004.

[33] The MathWorks, Inc. Partial Differential Equation Toolbox User's Guide. http://www.mathworks.com
14th June 2005

[34] Roger Y. Tsien. The green fluorescent protein. *Annu. Rev. Biochem.*, 67:509–544, 1998.